The University Of Alabama In Huntsville

College of Science
Computer Science Department

Huntsville, Alabama 35899
Phone: (205) 895-6088

To: Research Administration

From: John Ziebarth, Department of Computer Science

Date: April 1, 1994

RE: Final Report for FNAS CFD Combustion Annalysis NAS 8-38609 D.O. 56 (5-33074)

Enclosed is the final report for the above referenced contract. It has been under development by the investigators at The University of Alabama in Huntsville and Marshall Space Flight Center.

A Combined Eulerian-Volume of Fraction-Lagrangian Method for Atomization Simulation

Final Report

Contract No: NAS 8-38609 D.O. 56

By

S.P. Seung, C.P. Chen, and J.P. Ziebarth

University of Alabama in Huntsville,
Huntsville, AL 35899

Period Performance: Nov.1992 - Nov.1993

For

CFD Branch (ED32)
NASA-Marshall Space Flight Center

Table of contents

1. Introduction

The atomization and breakup process of liquid fuel jet is of vital importance to combustion performance of many practical devices, such as liquid rocket engines, gas-turbine combustors and diesel engines. In SSME or STME, for example, non uniform mixing of the liquid oxygen/hydrogen propellants in the atomization processes is responsible for the injector performance loss and influences the consequent evaporation, gas-gas mixing and combustion, and combustion instability.

Numerical modeling of liquid-jet atomization requires the resolution of the different conservation equations that describe the dynamics of the interfaces separating two immiscible fluids as well as the droplet/spray dynamics due to the breakup of liquid droplets from the liquid-gas interface. Past atomization models [1,2] have relied highly on the simple one-dimensional idealized model [3,4] or using empirical formulation based on specific injectors.

During the last decade, general multiphase computational fluid dynamics methodologies have matured to the point that several attempts have been made to model the detailed atomization process. Reitz [5] has developed an "Blob Injection" atomization model based on wave instability analysis. This model has been casted in the KIVA code for diesel engine applications[6] and also been used by Kim et al. [7,8,9] to study combustion instability of a annular liquid combustor model Habiballah et al. [10]. Przekwas and co-workers [11] have used direct numerical simulation to study the instability and breakup of laminar jets and have device a "jet embedding" technique to couple with flow solvers for liquid-engine thrust chamber calculations. Probably the most rigorous numerical modeling of atomization process are the works done by Liang and co-workers [12,13,14,15].

The ARICC-3D code developed by them combined the volume of fluid (VOF) methodology with the spray combustion code KIVA II. The VOF method is used for tracking two immiscible fluids and the resulting spray/droplets and combusting gas are solved by Lagrangian particle tracking and ALE/ICE (Arbitrary Lagrangian-Eulerian/Implicit Continuous Eulerian) finite volume differencing of the reacting flow equations. The ARICC-3D enables the simultaneous treatments of three phases: a compressible gaseous mixture, an incompressible liquid, and a dispersed droplet spray. Recent applications [15] involve a single element injector analysis and a multi-element injector analysis to study the combustion

response to a bomb blast with and without baffles. The multi-element computations were found very time-consuming. The authors lists several areas where effort has to be made to enhance the computational efficiency. One of the improvement which they made recently is to recast the VOF formulation into a pressure-based flow solver based on the SIMPLE algorithm [16].

In the last few years, we have used the state-of-art pressure based method, the PISOC algorithm, for calculating chemical reacting flows at all speeds involving spray combustion [7,8,9,17,18]. Various physical models including the non-isotropic algebraic stress model (ASM), the multi-scale model, equilibrium and finite rate chemistry, turbulent modulation due to droplets, group droplet dispersion due to turbulence, droplet coalescence and breakup have been incorporated into the current MAST code [19,20].

The MAST code uses primitive variables on a non-staggered general curvilinear grid system and follows the PISOC algorithm on a time-marching scheme. One predictor-muticorrector sequence was formulated within each time step for time-accurate transient calculations. The Chakravarthy-Osher's high order scheme [21] was used for the convection terms in the governing equations and the conjugate-gradient (CGS) matrix solver was used for solving the descretized algebraic equations sequentially for each variables with the predictor-corrector sequence. The purpose of this study is to extend this algorithm to involve volume-displacement effect encountered in very dense region in the primary atomization regions. The fractional volume of fluid (VOF) method will be coupled with the existing Eulerian-Lagrangian scheme currently used in the MAST code to resolve three phases: an incompressible liquid fuel phase, a compressible gas phase, and a dispersed droplet phase, within the calculation domain. To calculate the surface tension effect, we used the continuum surface force (CSF) model [22,23]. This model interprets surface tension as a continuous, three-dimensional effect across an interface, rather than as a boundary condition on the interface. The continuum method eliminates the need for interface reconstruction, and simplifies the calculation of surface tension.

In this study, to verify the tracking of free surfaces between liquid and gas phases and to analyze the interfacial phenomena between liquid and gas phases, we assume the gas and liquid phases are incompressible. The confined dam broken problem and water sloshing problem were carried out. Also, to verify the surface tension force effects, the single droplet problem and the jet breakup problem were solved. Detailed formulation and validation will be described in the following sections.

2. Governing Equations and Physical Models

2-1. Governing Equations

The mathematical formulations for the three-phases (liquid, gas, and droplet phase) flow and combustion processes comprise the Eulerian conservation equations for the liquid and gas phases and Lagrangian equations for the fuel droplets. The link between three phases is mathematically expressed in terms of the interaction source terms in the governing equations [19]. The tracking of the free surface between the liquid and gas phase is represented by the VOF method.

All phases processes are modeled by a system of unsteady, multi-dimensional equations. The gas and liquid phases are written in Eulerian coordinates whereas the liquid-droplet phase is presented in Lagrangian coordinates. The two-way coupling between the two phases is described by the interaction source terms which represent the rates of momentum, mas and heat exchange. The detailed equations can be found in ref. 19. The current method is intended to predict the motion of the fluid interfaces based on the use of a conserved scalar variable transport equation. The conserved scalar is the fractional volume of fluid (VOF) cell partitioning function, and the solution of which provides information on the position and shape of the interface [24,25]. Through a linear relation, it also determine the fluid properties. By defining the fractional volume in a typical control volume cell:

$$F = \frac{V_l}{V_g + V_l} \tag{2-1}$$

where V represents volumes occupied by gas phase (V_g) or liquid phase (V_l) within the control volume considered. In the absence of interfacial heat and mass transfer, the function F obeys the volume flux conservation equation:

$$\frac{\partial F}{\partial t} + \frac{\partial}{\partial x_i}(u_i F) = 0 \tag{2-2}$$

For this initial study, by assuming both liquid and gas flows are incompressible, all other conservation equations can be expressed in terms of volume of fraction F. These are

continuity equation,

$$\frac{\partial \bar{\rho}}{\partial t} + \frac{\partial}{\partial x_i}(\bar{\rho}\, u_i) = 0 \tag{2-3}$$

and momentum conservation equation,

$$\frac{\partial \bar{\rho} u_i}{\partial t} + \frac{\partial}{\partial x_j}(\bar{\rho} u_i u_j) = -\frac{\partial p}{\partial x_i} - \frac{\partial}{\partial x_i}(\frac{2}{3}\rho\bar{\kappa}) + \frac{\partial}{\partial x_j}\tau_{ij} + g_i + F_{sv} \tag{2-4}$$

where $\bar{\rho}$ is the averaged density defined as;

$$\bar{\rho} = \rho_l F + (1 - F)\, \rho_g \tag{2-5}$$

and, g_i is the body force (gravity), F_{sv} is the volume force for the surface tension effects, and $\bar{\kappa}$ is the turbulent kinetic energy and the viscous stress tensor is

$$\tau_{ij} = \mu \left[\frac{\partial u_i}{\partial x_j} + \frac{\partial u_j}{\partial x_i} - \frac{2}{3}\frac{\partial u_k}{\partial x_k}\delta_{ij} \right] \tag{2-6}$$

2-2. Physical Models

To analyze the atomization of liquid rocket engine and spray combustion, it is necessary to incorporate the knowledge and concepts of liquid-gas, droplet-gas, and liquid-droplet-gas interfacial phenomena and modeling for resolving the liquid volumes displacement effects. To resolve the dynamics of the interfaces separating two immisciable fluids, the tracking of free surfaces has to be considered.

In the present study, the free-surface tracking procedure to analyze the interfacial phenomena between the liquid and gas-phase in atomization and spray combustion is represented by the volume of fraction (VOF) method. And also, for the calculation of surface tension force, the continuum surface force (CSF) model [22,23] is used. The various physical models including the non-isotropic algebra stress model (ASM), the multi-scale model,

equilibrium and finite rate chemistry, turbulent modulation due to group droplet dispersion, droplet coalescence and breakup can be found in refs. 7,8,9,17 for details.

a. VOF Method for Tracking the Free Surface

In fluid dynamics, Lagrangian and Eulerian coordinates have been used to the tracking of free surfaces. In the first approach using Lagrangian discrete representation of a fluid with free surface, each zone of grid that subdivides the fluid into elements remains identified with the same fluid element for all time. In this case, the grid moves with the computed element velocities. It has the advantage of circumventing the problem of numerical diffusion across the interface. However, the methods become inapplicable whenever the deformation of the interface is severe, such as in droplet and liquid jet breakup studies.

The second method seeks to retain the numerical versatility of a purely Eulerian representation. However, the convective flux calculation requires an averaging of the flow properties of all fluid elements that fluid themselves in a given mesh cell after some period of time. The convective averaging results in a smoothing of all variations in flow quantities, and in particular, a smearing of surfaces of discontinuity such as free surfaces. The only way to overcome this loss in boundary resolution is to introduce some special treatment that recognizes a discontinuity and avoids averaging across it.

One of the special treatments is the VOF (Volume of Fraction) method. This method was developed by the Los Alamos Group [24,25]. This method forms the basis of the SOLA-VOF program [25]. The SOLA-VOF solution algorithm has been designated for a wide range of applications. It may be applied to problems involving a single fluid having any number of free surfaces, or to two immiscible fluids separated by any number of free interfaces. In this technique, a function F(x,y,t) is defined whose value is unity at any point occupied by fluid and zero elsewhere. In particular, a unity value of F corresponds to a cell full of fluid, whereas a zero value indicates that the cell contains no fluid cells with F values between zero and unity contain a free surface.

Let F(x,y,t) stands for a conserved scalar variable of the fluid that define the fractional volume in a typical control volume cell (Eq.(2-1)). That is, free surface reconstructed by means of a conserved scalar variable F(x,y,t), where

$$F(x,y,t) = \begin{cases} 1 & : \text{in the liquid phase} \\ 0 < F(x,y,t) < 1 & : \text{at the free surface} \\ 0 & : \text{in the gas phase} \end{cases} \qquad (2\text{-}7)$$

Consider at a fixed point r_o in space, we can obtain F as a function of time and can therefore calculate the rate of change $\partial F/\partial t$ at this point. From this limited knowledge of F we have no way of knowing, how F changes with time if we stay with a particular particle and following it along as it passes through the point at r_o. To find this Lagrangian rate of change we need to relate the value of F at r_o at time t_o to its value at a neighboring point $r_o + dr$ at time t_o+dt, where $dr = v\,dt$ is a small displacement along the flow line passing through the point at r_o. Now F has the value $F_o = F(x_o, y_o, t_o)$ at r_o at time t_o. When a particle at this point at the time t_o arrives at the neighboring point at the time t_o+dt, the function F has the value

$$F(x_o+d\xi, y_o+d\eta, t+dt) \qquad (2\text{-}8)$$

$$= F_o + \left(\frac{\partial F}{\partial x}\right)_o d\xi + \left(\frac{\partial F}{\partial y}\right)_o d\eta + \left(\frac{\partial F}{\partial t}\right)_o dt \qquad (2\text{-}9)$$

Where, ξ and η represent the displacement in the direction of x and y respectively. The total increment in F is therefore

$$dF = \left(\frac{\partial F}{\partial x}\right)_o d\xi + \left(\frac{\partial F}{\partial y}\right)_o d\eta + \left(\frac{\partial F}{\partial t}\right)_o dt \qquad (2\text{-}10)$$

Hence, the time rate of change of F from the Lagrangian viewpoint is

$$\frac{dF}{dt} = \left(\frac{\partial F}{\partial x}\right)_o \frac{\partial \xi}{\partial t} + \left(\frac{\partial F}{\partial y}\right)_o \frac{\partial \eta}{\partial t} + \left(\frac{\partial F}{\partial t}\right) \qquad (2\text{-}11)$$

The conserved scalar variable F(x,y,t) is governed by the following transport equation

$$\frac{\partial F}{\partial t} + u_i \frac{\partial F}{\partial x_i} = 0 \qquad (2\text{-}12)$$

where F(x,y,t) at time t=0 has to be given. Although the Eq.(2-12) is obtained by the particular point and at a particular time, both position and time and arbitrarily chosen; this

Eq.(2-12) constitutes a general kinematical relation that always holds for a fluid. However, in this study, by assuming both liquid and gas flows are incompressible. Eq.(2-12) can be written in the form of Eq.(2-2)

When the VOF equation is solved over a computational cell, the changes in F in a cell reduce to fluxes of F across the cell faces. As previously noted, to calculate VOF value, we need a special numerical technique in computing these flux to reserve the sharp definition of free boundaries. Several researchers have previously used variations of this approach for tracking material interfaces. In SOLA-VOF [25], donor-acceptor flux approximation was used. The basic idea of this method is to use information about F downstream as well as upstream of the flux boundary to establish a crude interface shape, and then to use this shape in computing the flux. In ref. [26], the Van-Leer method was used to reduce the numerical diffusion and to calculate the flux accurately. In this present studies, the higher order Chakravarthy-Osher scheme [21] is used to solve the VOF equation.

b. CSF Model for Surface Tension Force.

Liquid surfaces are in a state of tension, as though they possessed an elastic skin, because fluid molecules at or near the surface experience uneven molecular forces of attraction. Since abrupt changes in molecular forces occur when fluid properties change discontinuously, surface tension is an inherent characteristic of material interfaces. Surface tension results in microscopic, localized "surface force" that exerts itself on fluid elements at interfaces in both the normal and tangential directions. Fluid interfacial motion induced by surface tension plays a fundamental role in many natural and industrial phenomena [23].

The free boundary between the liquid and gas is known as the interfacial region or, simply the interface. The interface region is that thin layer surrounding a geometric surface of separation, within which the physical properties differ noticeably from those in either of the bulk phases. The thickness of this layer is ill-defined because the variation of physical properties across it is continuous. To calculate the surface effects at the interfaces between two immiscible fluids, previous researcher adopt an approximation in which the interface is infinitely thin; that is, they regard the phase boundary as a geometry surface, and assume that the properties right up to the interface are unchanged from those of the respective bulk phase. An alternative description from an energetic point of view follows from the fact that because a liquid molecule at a liquid-gas interface must be attracted to less neighboring molecules than one in the interior of the fluid, the attractive energy per molecule at the surface

must then be some fraction of that in the interior. The energy of a surface molecule is therefore higher than that of one in the bulk liquid, so energy must be expended to move a molecule from the interior to the surface. However, since the free energy of the system will tend toward a minimum, the surfaces of the liquid phase tend to contact. With σ the force per unit length tending to contract the surface, we may therefore write that, at constant temperature and volume for a given number of moles of system,

$$\sigma = \frac{\partial G}{\partial A} \tag{2-13}$$

where, G represents the free energy and A represents surface area. The quantity σ is called the surface tension and is usually given in units of force per unit length. For a liquid-gas interface problem, there is an imbalance of intermolecular forces, although smaller. the magnitude of the interfacial tension usually lies between the surface tensions of each liquid. And, there will be a tendency to curve the interface, as a consequence of which there must be a pressure difference across the surface with the highest pressure on the concave side. The expression relating this pressure difference to the curvature of the surface is usually referred to as the Young-Laplace Equation. From a calculation of the P-V work required to expand the curved surface and so change its surface area, it is relatively straightforward to show that this equation may be written as

$$\Delta P = \sigma \left(\frac{1}{R_1} + \frac{1}{R_2} \right) \tag{2-14}$$

where R_1 and R_2 are the radii of curvature of the surface along any two orthogonal tangents (principal radii of curvature), and ΔP is the difference in fluid pressure across the curved surface. Note that the individual contribution of either R_1 or R_2 to the pressure difference is negative when moving radially outward from the corresponding center of curvature. As Eq.(2-14) is written, it is applicable to arbitrarily shaped surfaces where the radii of curvature may change spatially.

However, Eq.(2-14) has suffered from difficulties in modeling topological complex interface having surface tension. In this study, surface tension at free surface is modeled with a localized volume force prescribed by the recent CSF (continuum surface force) model. In CSF model, instead of a surface tensile force or a surface pressure boundary condition applied at a discontinuity, a volume force due to surface tension acts on fluid elements lying within

finite thickness transition regions replacing the discontinuities. CSF formulation makes use of the fact that numerical models of discontinuities in finite volume and finite difference scheme are really continuous transitions within which the fluid properties vary smoothly from one fluid to another. The volume force in CSF model is easily calculated by taking first and second order spatial derivatives of the characteristic data. In the case of theVOF method, it is the VOF function F. At each point within the free surface transition region, a cell-centered value F_{SV} is defined which is proportional to the curvature κ of the constant VOF surface at that point.

Surface tension modeled with the continuum method eliminates the need for interface reconstruction, so restriction on the number, complexity, or dynamic evolution of interfaces having surface tension are not imposed.

Surface Tension Force

The surface stress boundary condition at an interface between two fluid is

$$(P_1 - P_2 + \sigma \kappa)n_i = (\tau_{1ik} - \tau_{2ik})n_k + \frac{\partial \sigma}{\partial x_i} \qquad (2\text{-}15)$$

where σ is the fluid surface tension coefficient. P_1 and P_2 are the pressure in fluid(1 and 2). τ is the viscous stress term. κ is the free surface mean curvature. In this study, for the accurate modeling of the normal boundary condition for interface, we assumed that the viscosity at the interface is neglected and the surface tension coefficient is constant. Therefore, the fluid pressure jump across an interface under surface tension is

$$P_S = P_2 - P_1 = \sigma \kappa(x) \qquad (2\text{-}16)$$

where P_S is the surface pressure. Surface pressure is therefore proportional to the curvature of the interface. Surface tension contributes a surface pressure that is the normal force per unit interfacial area. Therefore, the surface force per unit interfacial area can be written as

$$F_{sa}(x) = \sigma \kappa(x)\vec{n} \qquad (2\text{-}17)$$

where $\vec{n}$ is the normal vector at the free surface. In the CSF model, the surface tension is reformulated as a volume force F_{SV} satisfying

$$\lim_{h \to 0} \int_{\Delta V} F_{sv}(x) d^3x = \int_{\Delta S} F_{sa}(x) ds \qquad (2\text{-}18)$$

and h is a length comparable to the resolution afforded by a computational mesh with spacing dx.(Fig.1) The area integral is over the portion ΔS of the surface lying within the small volume of integration ΔV. The finite difference approximation in MAST-VOF replace free surface discontinuities with finite thickness transition regions within which the fluid properties vary smoothly from fluid to gas over a distance of O(h).

$$F_{sv}(\mathbf{x}) = \sigma \kappa(\mathbf{x}) \frac{\nabla \tilde{F}}{[F]} \qquad (2\text{-}19)$$

where $\tilde{F}$ is the fluid characteristics, equal with the VOF value in MAST-VOF. When $\tilde{F}$= F, the volume force is computed accurately for any two fluids meeting at the interface. In particular, the two fluids could have equal densities. The mean free surface curvature κ , given by [22,23]

$$\kappa(x) = -\nabla \hat{n} = \frac{1}{|\vec{n}|}\left[\left(\frac{\vec{n}}{|\vec{n}|} \nabla \right) |\vec{n}| - (\nabla \vec{n}) \right] \qquad (2\text{-}20)$$

where the unit vector

$$\hat{n} = \frac{\vec{n}}{|\vec{n}|} \qquad (2\text{-}21)$$

is derived from a normal vector $\vec{n}$

$$\vec{n} = \nabla F \qquad (2\text{-}22)$$

that is the gradient of VOF data. The volume force, $F_{sv}(x)$ has the following properties;

(1). The volume force in the transition region in Fig.1, where there characteristic varies smoothly form fluid 1 to fluid 2, is designated to simulate the surface pressure on the interface between the fluids. Thus, the line integral of $F_{sv}(x)$

across the transition region is approximately equal to the conventional surface pressure:

$$\int_{p1}^{p2} F_{sv}(\mathbf{x})\, d(\hat{n}\cdot\mathbf{x}) = \int_{c1}^{c2} \sigma\, \kappa(\mathbf{x})\hat{n}(x)\frac{d\tilde{F}(\mathbf{x})}{[F]} \qquad (2\text{-}23)$$

$$\cong \sigma\, \kappa(\mathbf{x})\, \hat{n}\,(\mathbf{x}) \qquad \text{for } h > 0$$

(2). In the limit that the width of the transition region in a direction normal to the interface goes to zero, the volume force becomes the conventional surface pressure.

Modeling surface tension requires some special consideration, since the effects of surface tension should be confined to the neighborhood of the interface. To simplify the application of boundary conditions and to localize the domain of dependence of the volume force, an approximation with compact support is sought. To maintain the integrity of the transition region, the volume force should not change sign along the radius of curvature.

Because the contribution to the surface tension force come from the small portion of the computation mesh in the neighborhood of the interface, difficulty in formulating sufficiently accurate finite difference expression might be expected. It turns out that low-order approximations may be used, provided one begins with a form of the volume force that emphasizes the region of maximum gradient. This allows one to apply boundary conditions with no more difficulty than with other terms, such as pressure. In the CSF model for surface tension, a surface force is formulated to model numerically surface tension effects at fluid interface having finite thickness. The method is basically suited for Eulerian interfaces that are in general aligned with the computational grid. It can alleviate previous topological constraints on modeling interfaces having surface tension without sacrificing accuracy.

The CSF model has been validated on the single droplet problem at the equilibrium state. This problem will be described in the next section.

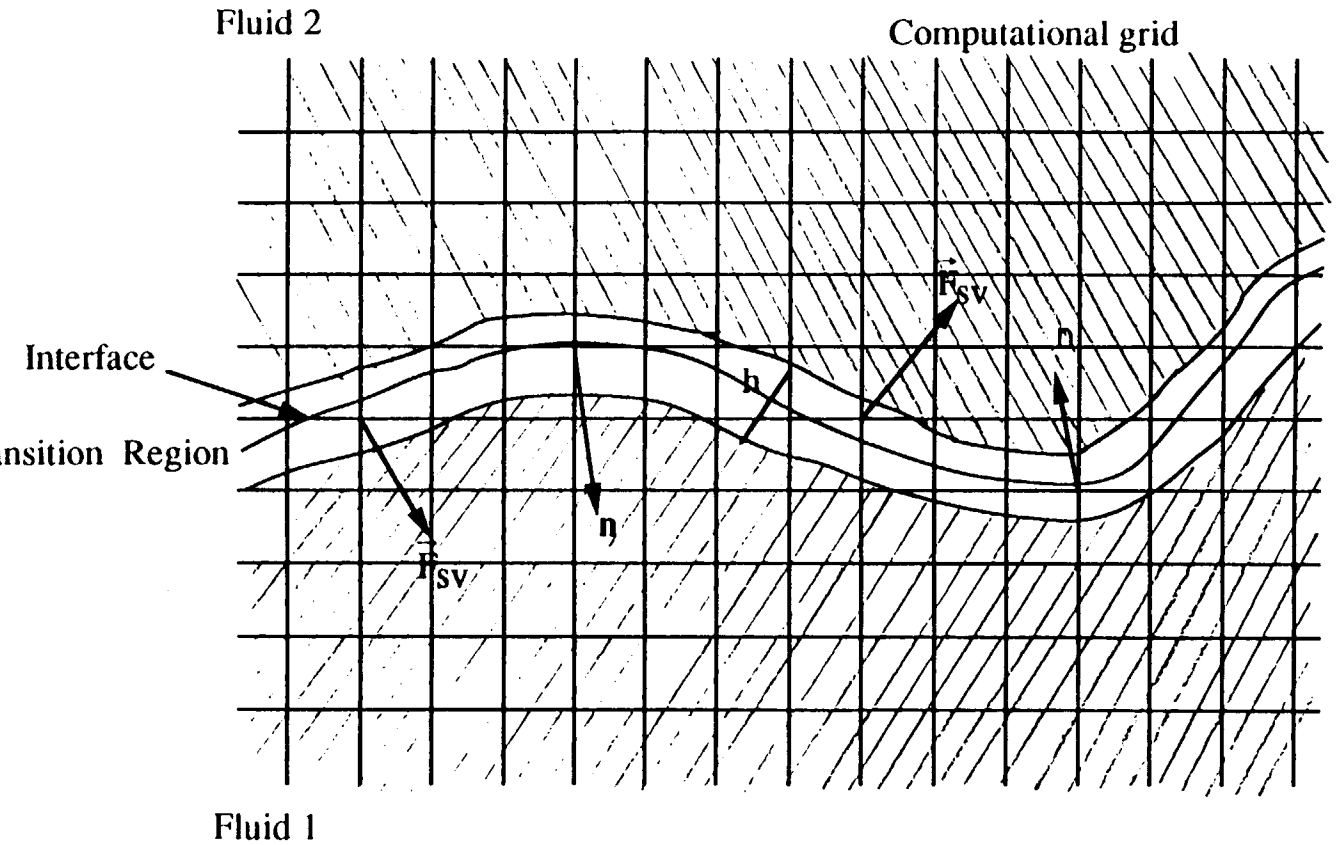

Fig.1 Schematic Diagram for Interface region

3. Finite Difference Equation

3-1. Finite Difference Equation for Transport Equations

The control volume method was used to derive the difference equations with all variables located at each cross point of a grid mesh. The grid system is shown in the Fig. 2, where the dash lines are the boundaries of control volume with east, west, north and south faces and P, E, W, N, S are grid main points. The transport equations are discretized by the Euler implicit difference scheme. The governing equations can be expressed in difference form for each grid point as

Continuity equation:

$$\frac{1}{\Delta t}\left[\rho^{n+1} - \rho^{n}\right] + \Delta_i (\rho U)^{n+1} = 0 \qquad (3\text{-}1)$$

Momentum equation:

$$\frac{1}{\Delta t}\left[(\rho U)^{n+1} - (\rho U)^{n}\right] = H'(U^{n+1}) - \Delta_i P^{n+1} + S_u + S_{st} + S_{bf} \qquad (3\text{-}2)$$

VOF equation

$$\frac{1}{\Delta t}\left[F^{n+1} - F^{n}\right] + \Delta_i (U_i F)^{n+1} = 0 \qquad (3\text{-}3)$$

In the above equations, the operators H' denotes the finite difference representation of the spatial convective and diffusive fluxes of velocity U_i, F stands for VOF value. The operator Δ_i represents the first order Euler finite difference of $\partial/\partial x_i$. The source terms, S_u, contains all other terms except the convective and diffusive term for each variables. S_{st} stands for the surface force due to surface tension. S_{bf} represents body force due to gravity.

In order for the solution procedure of the finite difference equations to be stable, the simplest way without losing accuracy is to separate the diagonal elements of the operators H' and to shift them to the left-hand side of the equations. The concentration is focused on the momentum equation:

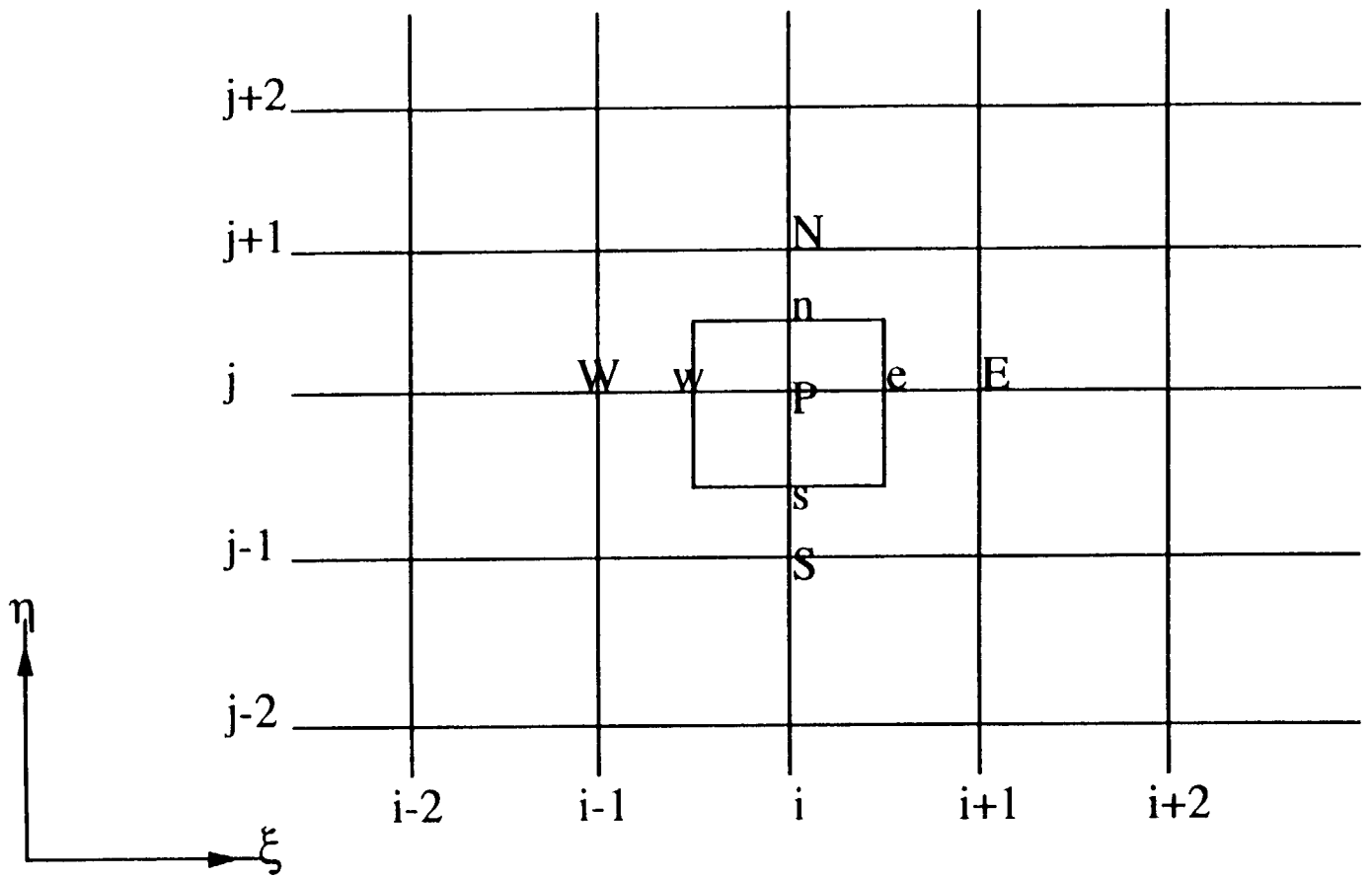

Fig. 2. Computational grid system

$$H'(U_i) = H(U_i) - A_p\, U_i \qquad (3\text{-}4)$$

where,

$\bar{H}$ operator of convection and diffusion term at neighbor points surrounding the main point p

A_p coefficient of the diagonal element of the operator H.

3-2. Finite Difference Equation for VOF Equation

In Eulerian representation, the convective flux calculation usually requires an averaging of the flow properties of all fluid elements in given mesh cells. This convective averaging results in a smoothing of all variations in flow quantities, and in particular, a smearing of surfaces of discontinuity such as free surfaces. To calculate the interface fluxes for the advection term, the upwind scheme is too dissipative, while the central and Lax-Wendroff schemes are too dispersive in the vicinity of discontinuities. To overcome this loss of accuracy in boundary resolution and to handle sharp interfaces between liquid and gas phases, a high accuracy scheme is implemented. This high accuracy scheme must have the ability to generate numerical algorithm which allow a high resolution of discontinuities, such as shock waves and contact discontinuities, without oscillation. In this study, to prevent the generation of numerical oscillations and to calculate the interface flues exactly at the interfaces between the liquid and gas, the Chakravarthy-Osher scheme [21] is used. This scheme is a kind of TVD (Total Variation Diminishing) scheme, whereby the variation of the numerical solution is controlled in a non-linear way, such that it forbids the appearance of any new extremum.. This scheme can be defined essentially in terms of one parameter. By various choices of this parameter, one can obtain schemes with a wide range of accuracy including high accuracy (low truncation error) second-order schemes, the conventional second-order accurate upwind TVD scheme and even a third-order accurate TVD scheme. This scheme can easily apply to scalar equations, to systems of equations, to arbitrary curvilinear coordinate systems, and to general control volumes.

The transport equation for the conserved scalar variable F can be transformed to a general curvilinear coordinate system. From Eq. (2-2), this equation can be written;

$$J\frac{\partial F}{\partial t} + \frac{\partial}{\partial \xi}(U F) + \frac{\partial}{\partial \eta}(V F) = 0 \qquad (3\text{-}5)$$

Where, U and V are the contra-variant velocity in the transformed coordinates.
Integrate with respect to the control volume in the grid system Fig.(1).

$$J\frac{F^{n+1} - F^n}{\Delta t} + |UF|_e - |UF|_w + |VF|_n - |VF|_s = 0 \tag{3-6}$$

In the above equation, the interface fluxes are calculated by using the Chakravarthy-Osher scheme. The F flux term in the direction of ξ is obtained as follow;

$$\frac{\partial}{\partial \xi}(UF) = \frac{\partial f}{\partial \xi} = \frac{f_{i+1/2,j} - f_{i-1/2,j}}{\Delta \xi} \tag{3-7}$$

then the control-volume interface flux is computed according to;

$$f_{i+1/2,j} = h_{i+1/2,j} + \frac{(1+\Phi)}{4} df^{+}_{i+1/2,j} - \frac{(1+\Phi)}{4} df^{-}_{i+1/2,j} + \frac{(1-\Phi)}{4} df^{+}_{i-1/2,j} - \frac{(1-\Phi)}{4} df^{-}_{i+3/2,j} \tag{3-8}$$

In the above, h represents a first-order numerical flux, and can be expressed

$$h_{i+1/2,j} = U^{+}_{i+1/2,j} F_{i,j} + U^{-}_{i-1/2,j} F_{i+1,j} \tag{3-9}$$

where

$$U^{\pm}_{i+1/2,j} = 0.5 \left(U_{i+1/2,j} \pm |U_{i+1/2,j}| \right) \tag{3-10}$$

The flux-limited values of df are computed as follows:

$$df^{+}_{i+1/2,j} = U^{+}_{i+1/2,j} \left(F^n_{i+1,j} - F^n_{i,j} \right) \tag{3-11}$$

$$df^{+}_{i-1/2,j} = U^{+}_{i+1/2,j} \left(F^n_{i,j} - F^n_{i-1,j} \right) \tag{3-12}$$

$$df^{-}_{i+1/2,j} = U^{-}_{i+1/2,j} \left(F^n_{i+1,j} - F^n_{i,j} \right) \tag{3-13}$$

$$df^{-}_{i+3/2,j} = U^{-}_{i+1/2,j} \left(F^n_{i+2,j} - F^n_{i+1,j} \right) \tag{3-14}$$

Also, the west, north, and south face fluxes can be obtained by a similar way.
The spatial accuracy of the scheme is controlled by the parameter Φ , which may take the following values:

$\Phi = -1$	Fully upwind scheme
$\Phi = -1/3$	No name scheme
$\Phi = 0$	Fromm scheme
$\Phi = 1/3$	Third order upwind scheme
$\Phi = 1/2$	Low truncation error second order scheme
$\Phi = 1$	Central difference scheme

3-3. Finite Difference Equation for Surface Tension Force

The CSF model for surface tension is implemented by placing the normal at grid main point and the curvature κ at cell centers as shown Fig.1. The shading part is the control volume for the computational domain.

From Eq.(2-19) and Eq.(2-20), the vector and the mean curvature also can be expressed

$$\vec{n} = \frac{\partial F}{\partial x}\, e_i + \frac{\partial F}{\partial y}\, e_j \tag{3-15}$$

$$\kappa(x) = \frac{1}{|\vec{n}|}\left[\left(\frac{n_x}{|\vec{n}|}\right)^2\left(\frac{\partial n_x}{\partial x}\right) + \left(\frac{n_x\, n_y}{|\vec{n}|^2}\right)\left(\frac{\partial n_x}{\partial y} + \frac{\partial n_y}{\partial x}\right) + \left(\frac{n_y}{|\vec{n}|}\right)^2\left(\frac{\partial n_y}{\partial y}\right)\right] \left[-\left(\frac{1}{r^\alpha}\frac{\partial}{\partial y}\left(r^\alpha\frac{\partial F}{\partial y}\right) + \frac{\partial}{\partial x}\left(\frac{\partial F}{\partial x}\right)\right)\right] \tag{3-16}$$

And the derivatives in above equations are transformed to a general form based on a non-orthogonal coordinate system (ξ, η). The first derivatives are as follows;

$$\frac{\partial F}{\partial x} = \xi_x \frac{\partial F}{\partial \xi} + \eta_x \frac{\partial F}{\partial \eta} \tag{3-17}$$

$$\frac{\partial F}{\partial y} = \xi_y \frac{\partial F}{\partial \xi} + \eta_y \frac{\partial F}{\partial \eta} \tag{3-18}$$

The second derivatives are as follows;

$$\frac{\partial}{\partial x}\left(\frac{\partial F}{\partial x}\right) = \xi_x \frac{\partial}{\partial \xi}(n_x) + \eta_x \frac{\partial}{\partial \eta}(n_x) \tag{3-19}$$

$$\frac{\partial}{\partial y}\left(\frac{\partial F}{\partial y}\right) = \xi_y \frac{\partial}{\partial \xi}(n_y) + \eta_y \frac{\partial}{\partial \eta}(n_y) \tag{3-20}$$

The cross derivatives are as follows;

$$\frac{\partial}{\partial x}\left(\frac{\partial F}{\partial y}\right) = \xi_x \frac{\partial}{\partial \xi}(n_y) + \eta_x \frac{\partial}{\partial \eta}(n_y) \tag{3-21}$$

$$\frac{\partial}{\partial y}\left(\frac{\partial F}{\partial x}\right) = \xi_y \frac{\partial}{\partial \xi}(n_x) + \eta_y \frac{\partial}{\partial \eta}(n_x) \tag{3-22}$$

And the second derivative for the cylindrical coordinate is as follow;

$$\frac{1}{r^\alpha}\frac{\partial}{\partial y}\left(r^\alpha \frac{\partial F}{\partial y}\right) = \frac{1}{r^\alpha}\left\langle \xi_y \frac{\partial}{\partial \xi}\left(r^\alpha \xi_y \frac{\partial F}{\partial \xi}\right) + \xi_y \frac{\partial}{\partial \xi}\left(r^\alpha \eta_y \frac{\partial F}{\partial \eta}\right) + \eta_y \frac{\partial}{\partial \eta}\left(r^\alpha \xi_y \frac{\partial F}{\partial \xi}\right) + \eta_y \frac{\partial}{\partial \eta}\left(r^\alpha \eta_y \frac{\partial F}{\partial \eta}\right)\right\rangle \tag{3-23}$$

Where,

$$n_x = \frac{\partial F}{\partial x} \tag{3-24}$$

$$n_y = \frac{\partial F}{\partial y} \tag{3-25}$$

and, the superscript α on the radius r is a constant equal to 1 in the cylindrical coordinate and 0 in the Cartesian coordinate. The finite difference equations for above derivatives are

based on the control volume in the grid system (Fig.2). The finite difference equations are as follows;

$$\left|\frac{\partial F}{\partial \xi}\right|_e = F_{i+1,j} - F_{i,j} \tag{3-26}$$

$$\left|\frac{\partial F}{\partial \xi}\right|_w = F_{i,j} - F_{i-1,j} \tag{3-27}$$

$$\left|\frac{\partial F}{\partial \eta}\right|_n = F_{i,j+1} - F_{i,j} \tag{3-28}$$

$$\left|\frac{\partial F}{\partial \eta}\right|_s = F_{i,j} - F_{i,j-1} \tag{3-29}$$

therefore, the first derivatives can be expressed

$$[n_x]_p = \left[\frac{\partial F}{\partial x}\right]_p = \frac{1}{2}\left\langle \xi_{x,e}\left[\frac{\partial F}{\partial \xi}\right]_e + \xi_{x,w}\left[\frac{\partial F}{\partial \xi}\right]_w + \eta_{x,n}\left[\frac{\partial F}{\partial \eta}\right]_n + \eta_{x,s}\left[\frac{\partial F}{\partial \eta}\right]_s \right\rangle \tag{3-30}$$

$$[n_y]_p = \left[\frac{\partial F}{\partial y}\right]_p = \frac{1}{2}\left\langle \xi_{y,e}\left[\frac{\partial F}{\partial \xi}\right]_e + \xi_{y,w}\left[\frac{\partial F}{\partial \xi}\right]_w + \eta_{y,n}\left[\frac{\partial F}{\partial \eta}\right]_n + \eta_{y,s}\left[\frac{\partial F}{\partial \eta}\right]_s \right\rangle \tag{3-31}$$

and, the second order derivatives are;

$$\left|\frac{\partial n_x}{\partial \xi}\right|_e = [n_x]_E - [n_x]_P \tag{3-32}$$

$$\left|\frac{\partial n_x}{\partial \xi}\right|_w = [n_x]_P - [n_x]_W \tag{3-33}$$

$$\left|\frac{\partial n_x}{\partial \eta}\right|_n = [n_x]_N - [n_x]_P \tag{3-34}$$

$$\left|\frac{\partial n_x}{\partial \eta}\right|_s = [n_x]_P - [n_x]_S \tag{3-35}$$

$$\left[\frac{\partial}{\partial x}\left\langle\frac{\partial F}{\partial x}\right\rangle\right]_p = \frac{1}{2}\left\langle \xi_{x,e}\left[\frac{\partial n_x}{\partial \xi}\right]_e + \xi_{x,w}\left[\frac{\partial n_x}{\partial \xi}\right]_w + \eta_{x,n}\left[\frac{\partial n_x}{\partial \eta}\right]_n + \eta_{x,s}\left[\frac{\partial n_x}{\partial \eta}\right]_s \right\rangle \tag{3-36}$$

Similarly, the second order derivative in the direction of y can be obtained;

$$\left[\frac{\partial}{\partial y}\left\langle\frac{\partial F}{\partial y}\right\rangle\right]_p = \frac{1}{2}\left\langle \xi_{y,e}\left[\frac{\partial n_y}{\partial \xi}\right]_e + \xi_{y,w}\left[\frac{\partial n_y}{\partial \xi}\right]_w + \eta_{y,n}\left[\frac{\partial n_y}{\partial \eta}\right]_n + \eta_{y,s}\left[\frac{\partial n_y}{\partial \eta}\right]_s \right\rangle \tag{3-37}$$

Also, the second order cross derivatives are obtained;

$$\left[\frac{\partial}{\partial x}\left\langle\frac{\partial F}{\partial y}\right\rangle\right]_p = \frac{1}{2}\left\langle \xi_{x,e}\left[\frac{\partial n_y}{\partial \xi}\right]_e + \xi_{x,w}\left[\frac{\partial n_y}{\partial \xi}\right]_w + \eta_{x,n}\left[\frac{\partial n_y}{\partial \eta}\right]_n + \eta_{x,s}\left[\frac{\partial n_y}{\partial \eta}\right]_s \right\rangle \tag{3-38}$$

$$\left[\frac{\partial}{\partial y}\left\langle\frac{\partial F}{\partial x}\right\rangle\right]_p = \frac{1}{2}\left\langle \xi_{y,e}\left[\frac{\partial n_x}{\partial \xi}\right]_e + \xi_{y,w}\left[\frac{\partial n_x}{\partial \xi}\right]_w + \eta_{y,n}\left[\frac{\partial n_x}{\partial \eta}\right]_n + \eta_{y,s}\left[\frac{\partial n_x}{\partial \eta}\right]_s \right\rangle \tag{3-39}$$

These discretized equations are then substituted into Eq. (3-2) for calculating body forces based on the CSF model.

4. Numerical procedure

In this study, the basic algorithm for flow solver is the PISOC algorithm [20], which is based on the operator-splitting technique originally proposed by Issa [28], that is, the pressure implicit with splitting of operators (PISO) algorithm. PISO algorithm is a non-iterative method for handling the coupling of the implicitly discretized time-dependent single phase fluid flow and heat transfer. The PISO algorithm has been extended to include a stochastic Lagrangian particle tracking scheme for computing time-dependent gas-droplet flows [28]. Since for this study both gas and liquid phase are assumed incompressible, the variation of density is solely accounted for by the VOF information. By substituting the volume flux conservation equation (2-2) into the continuity equation (2-3). It can be shown the continuity equation retains the original incompressible form. Thus the same procedure described in [28] can be used here with an addition of a F-equation corrector step at the end of the last momentum corrector step. Special attention was paid to the solution of the F-equation.

4-1. PISO-VOF Algorithm

PISO algorithm is a non-iterative method for handling the coupling of the implicitly time dependent fluid flow equations. This algorithm is based on the use of pressure and velocity as dependent variables and is hence applicable to both the compressible and incompressible versions of the transport equations. The main feature of the technique of the splitting of the solution process into a series of steps whereby operations on pressure are decoupled from those velocity at each step, with the split sets of equations being amenable to solution by standard techniques. At each time-step, the procedure yields solutions which approximate the exact solution of the difference equations. The accuracy of this splitting procedure is assessed for a linearised form of the discretized equations, and the analysis indicates that the solution yielded by it differs from the exact solution of the difference equations by terms proportional to the powers of the time-step size. Detailed PISO algorithm and the PISOC algorithm can be found in Ref. [20,28] for dispersed multiphase reacting flows. The implementation of the VOF is summarized in the following;

Predictor Step

The equation of momentum is solved in this step implicitly, using old time pressure and density, as

$$\left(\frac{1}{\Delta t} + A_p\right) U_i^* = H(U_i^*) - \frac{1}{\rho}\Delta_i p^n + \frac{U_i^n}{\Delta t} + S_{u_i} \qquad (4\text{-}1)$$

The solution in this step yields U_i^*. velocity field. But, in this step, U_i^* velocity field will not in general satisfy the zero-divergence condition.

The equation of VOF is solved in this step also implicitly, using U_i^* and old time VOF value F^n, as

$$\left(\frac{1}{\Delta t} + A_p\right) F^* = G(F^*) + \frac{F^n}{\Delta t} \qquad (4\text{-}2)$$

where, G term is convective term for VOF.

First Corrector Step

In this step, the momentum equation can be written in the explicit corrector form

$$\left(\frac{1}{\Delta t} + A_p\right) U_i^{**} = H(U_i^*) - \frac{1}{\rho}\Delta_i p^* + \frac{U_i^n}{\Delta t} + S_{u_i} \qquad (4\text{-}3)$$

which, by subtracting predictor equation from it, and then combining the continuity equation and equation of state, the pressure increment equation can be obtained;

$$U_i^{**} = U_i^* - \frac{1}{\rho}\Delta_i \left(p^* - p^n\right) \qquad (4\text{-}4)$$

$$\left[\Delta_i \left(\frac{1}{\rho} D_u \Delta_i\right)\right]\left(p^* - p^n\right) = \Delta_i U_i^* \qquad (4\text{-}5)$$

This equation yields P^* field. Form Eq.(4-3), U_i^{**} can be obtained. The equation of VOF is solved in this step also explicitly, using U_i^{**}, F^*, and old time VOF value F^n, as follows;

$$\left(\frac{1}{\Delta t} + A_p\right) F^{**} = G(F^*) + \frac{F^n}{\Delta t} \qquad (4\text{-}6)$$

Second Corrector Step

For this step, the momentum corrector equation is

$$(\frac{1}{\Delta t} + A_p)\ U_i^{***} = H(U_i^{**}) - \frac{1}{\rho}\Delta_i p^{**} + \frac{U_i^n}{\Delta t} + S_{U_i}. \tag{4-7}$$

Also, in this step, the increment equation for momentum can be obtained as like the first corrector step;

$$(\frac{1}{\Delta t} + A_p)(U_i^{***} - U_i^{**}) = H(U_i^{**}) - H(U_i^{*}) - \frac{1}{\rho}\Delta_i (p^{**} - p^{*}) \tag{4-8}$$

Denote

$$D_u = (\frac{1}{\Delta t} + A_p)^{-1} \tag{4-9}$$

Thus,

$$U_i^{***} = U_i^{**} + D_u[(H(U_i^{**}) - H(U_i^{*})) - \frac{1}{\rho}\Delta_i (p^{**} - p^{*})] \tag{4-10}$$

Substitute U_i^{***} into the continuity equation, we obtain

$$[\Delta_i (\frac{1}{\rho} D_u \Delta_i)](p^{**} - p^{*}) = D_u \Delta_i[H(U_i^{**}) - H(U_i^{*})] \tag{4-11}$$

The above equation yields P^{**}, and then the other variable, U^{***}, ρ^{**} can be obtained. And, also the VOF value is obtained as follows;

$$(\frac{1}{\Delta t} + A_p)\ F^{***} = G(F^{**}) + \frac{F^n}{\Delta t} \tag{4-12}$$

4-2. The Construction of Free Surface

In this study, it is assumed that the boundary can be constructed by a straight line cutting through the cell By determining the slope of this line, it can then be moved across the cell to a position that intersects the known amount of F volume in the cell and neighborhood cells.

To determine the free surface position in the cell, first calculate the gradient of volume of fraction in the cell which has the value of volume of fraction greater than 0.5, that is, ∇F

$$\nabla F = \frac{\partial F}{\partial X_{i,j}} \mathbf{e}_i + \frac{\partial F}{\partial y_{i,j}} \mathbf{e}_j \tag{4-13}$$

and then, calculate the resultant of ∇F;

$$|\nabla F| = \sqrt{(\frac{\partial F}{\partial X})^2_{i,j} + (\frac{\partial F}{\partial y})^2_{i,j}} \tag{4-14}$$

The x-position and y-position of the free surface can approximately obtained from Eq.(4-13) and Eq.(4-14) ;

$$X_{sf} = x_{i,j} + (0.5 - F_{i,j}) (\frac{\partial F/\partial x}{|\nabla F|})_{i,j} \tag{4-15}$$

$$Y_{sf} = y_{i,j} + (0.5 - F_{i,j}) (\frac{\partial F/\partial y}{|\nabla F|})_{i,j} \tag{4-16}$$

By the similar way, the x and y positions of the neighborhood cells (i-1,j),(i,j-1) and (i+1,j) are obtained. And then , if $F_{i,j}$ is greater than 0.5 , $F_{i+1,j}$ is also greater than 0.5, and $F_{i,j+1}$ is less than 0.5, connect the point (X_{sf} , Y_{sf}) of the left-side cell (i-1,j) and the point (X_{sf} , Y_{sf}) of the left-side cell (i,j). In this case, The free surface is constructed horizontally. if $F_{i,j}$ is greater than 0.5 , $F_{i+1,j}$ is also less than 0.5, and $F_{i,j+1}$ is greater than 0.5, connect the point (X_{sf} , Y_{sf}) of the top-side cell (i,j) and the point (X_{sf} , Y_{sf}) of the bottom-side cell (i,j-1). In this case, The free surface is constructed vertically.

5. Validation

To validate the MAST-VOF, we solved dam broken problem, water sloshing problem, single droplet, and liquid column breakup problem. All problems were solved simultaneously liquid and gas phase.

5-1. Dam Broken Problem

In this calculation, a rectangular column of water in hydrostatic equilibrium is confined the wall as shown Fig. 3. At the beginning of the process the right wall is suddenly removed, the water column therefore starts to collapse, under the influence of gravity and to form an advancing water wave.

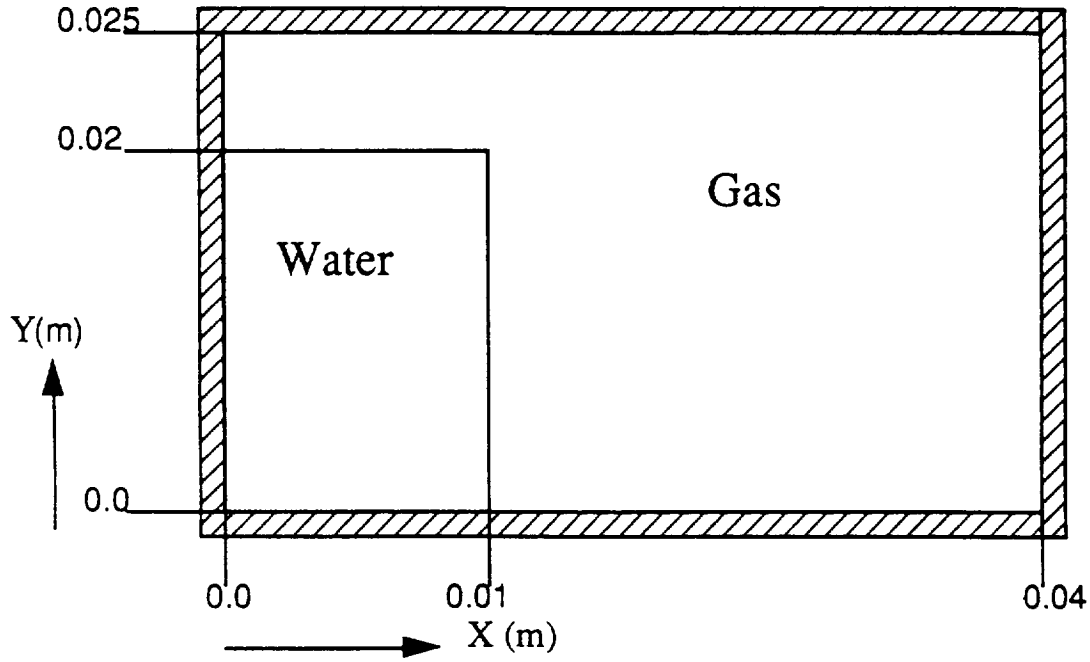

Fig.3 Schematic Diagram for Dam Broken Problem

This is a good test problem for tracking the free surface because it has simple boundary conditions and a simple initial configuration. The appearance of both a vertical and horizontal free surface, however, provides a check on the capability of MAST-VOF to treat free surface that are not single valued with respect to X-Y coordinate. The physical properties are listed in Table 1.

Table 1. Physical properties for dam broken problem

o Liquid physical properties
density : 1000.0 Kg/m^3
viscosity : 1.0 E-3 Kg m/sec
o Gas physical properties
density : 1.0 Kg/m^3
viscosity : 1.8 E-5 Kg m/sec
o Gravity : 0.01 m/sec^2

At the start of the calculation, VOF value F has the unit in the region occupied by the water, and zero in the gas phase. Also, the velocity components u and v are zero at the flow domain boundary. For the calculation, a grid consisting of 41x41 uniformly spaced cells has been chosen. The numerical results are shown in Fig. 4. At the initial state, there is no gas flow. When the dam collapse, the gas velocity was induced due to the momentum transfer from the liquid phase (water). Gas started to move from left to right wall. As the water front moves from left to right, the gas velocity increased and the recirculating flow also induced. Numerical results from the present method in terms of VOF values are in good agreement with those in ref. [26]. Also, the computed results of water column height H and wave front length Z are compared with the experimental data of Martin & Moyce [29] as shown in Table 2. From this comparison, it is seen that the present mathematical model is capable of tracking the free surface between the liquid and gas phase.

Table 2 Comparison of numerical results to experimental data

	MAST-VOF		Experimental Data	
Time(sec)	Z(cm)	H(cm)	Z(cm)	H(cm)
0.0	1.0	2.0	1.0	2.0
0.9	1.514	1.68	1.5	1.7
1.4	2.17	1.37	2.17	1.37
2.0	3.28	1.062	3.1	1.1

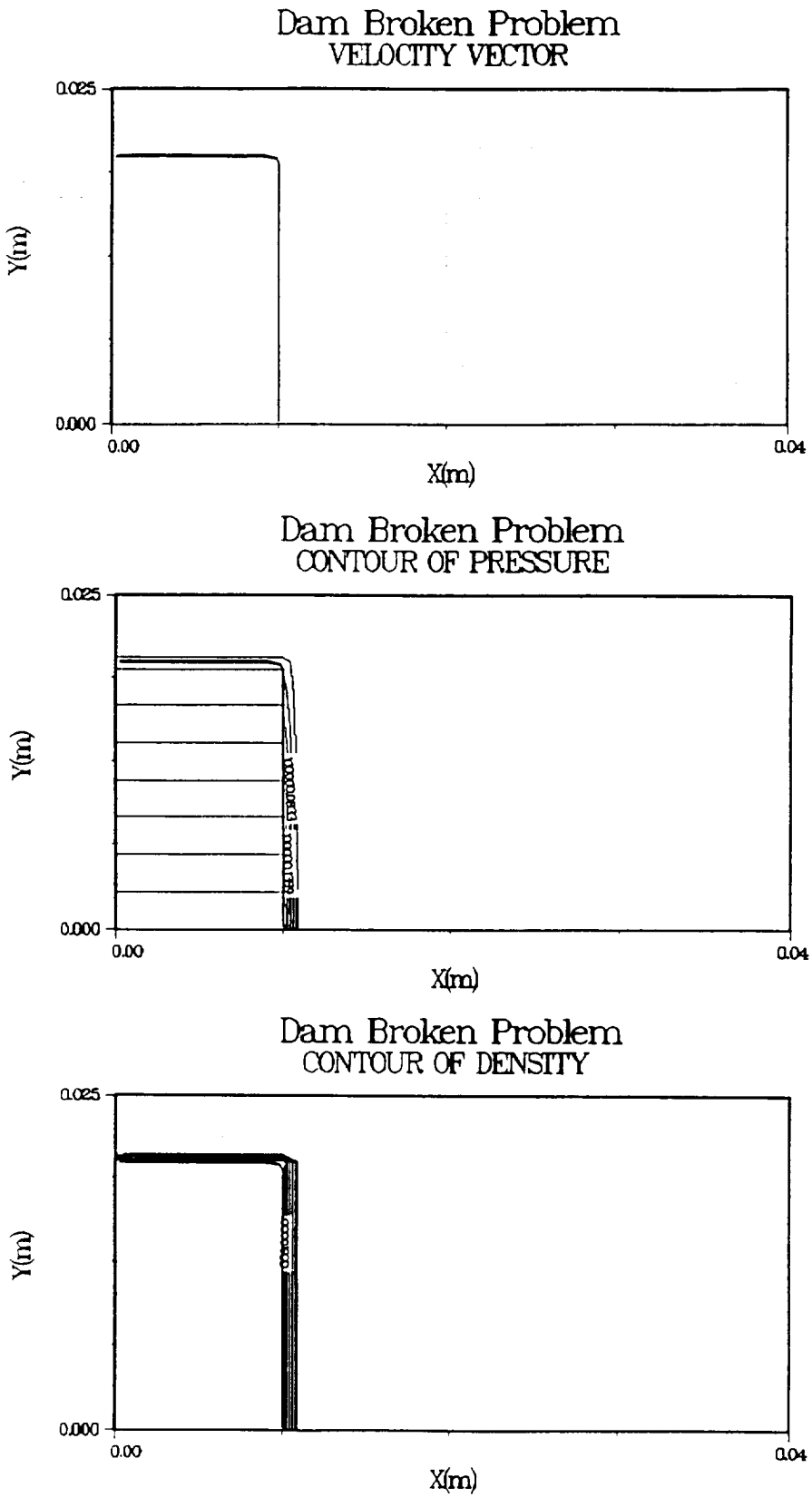

Fig. 4 Computational results for dam broken problem at time = 0.0 sec

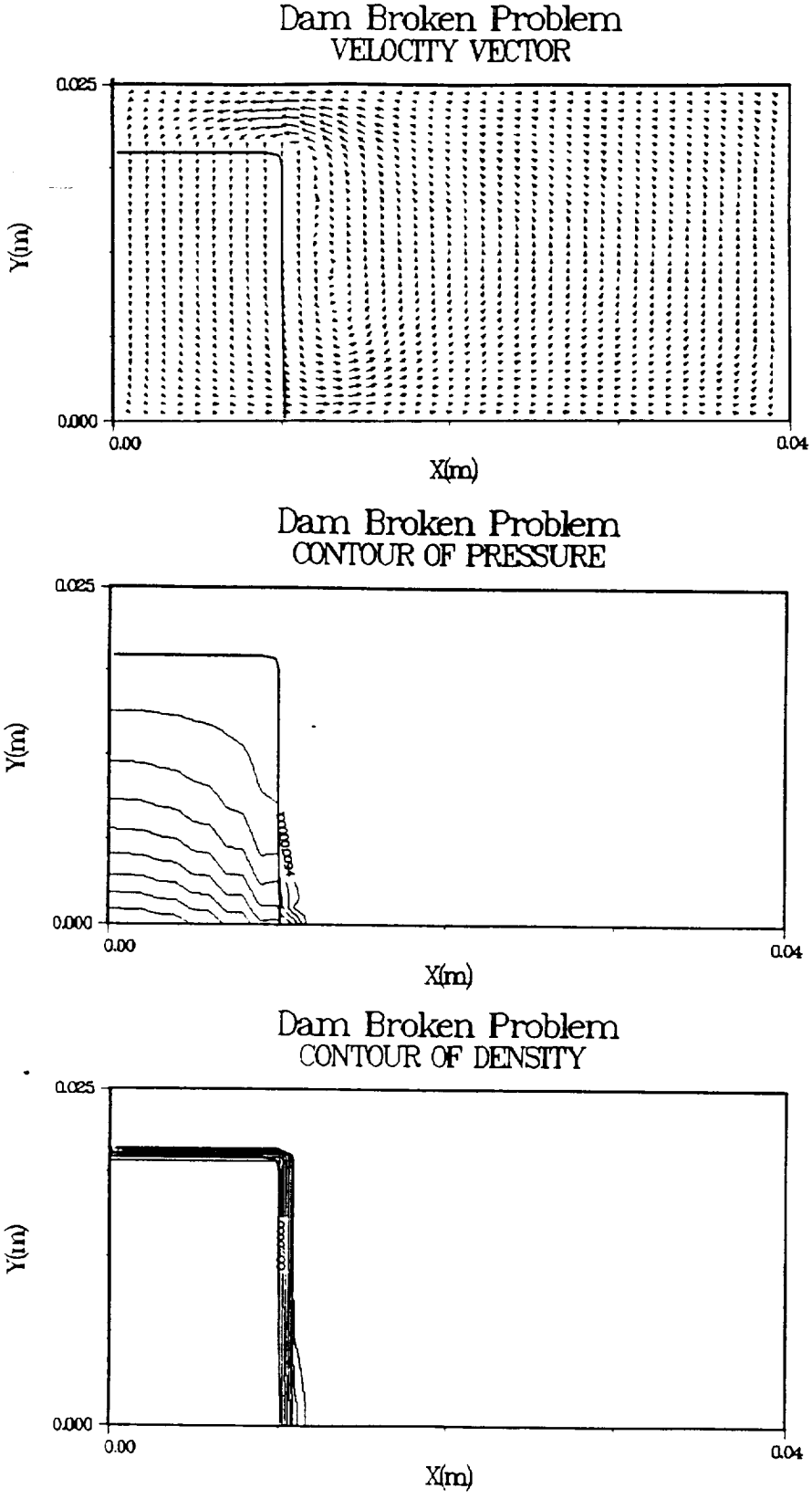

Fig. 4 Continue (at time = 0.2 sec)

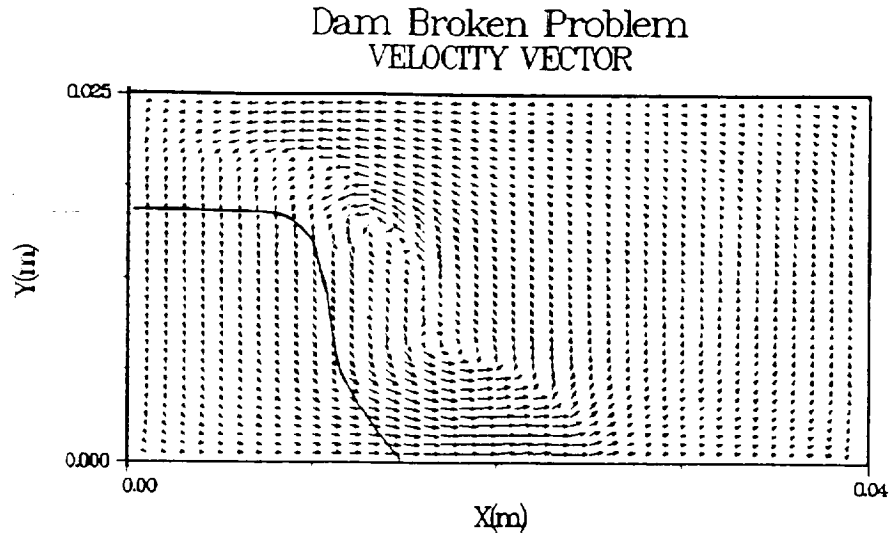

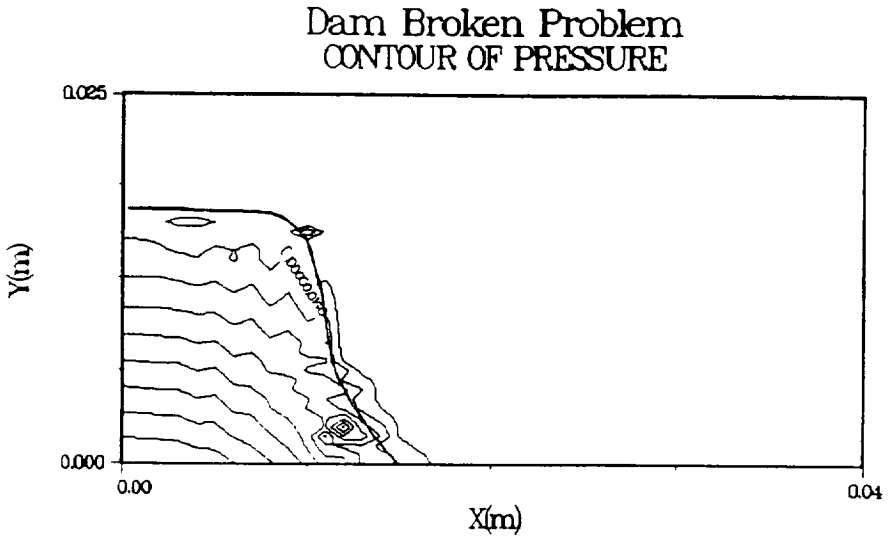

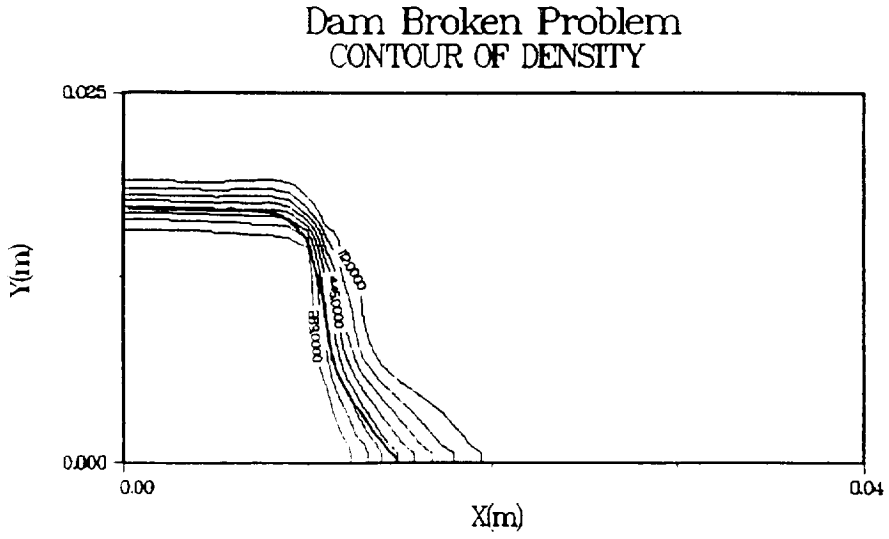

Fig. 4 Continue (at time = 0.9 sec)

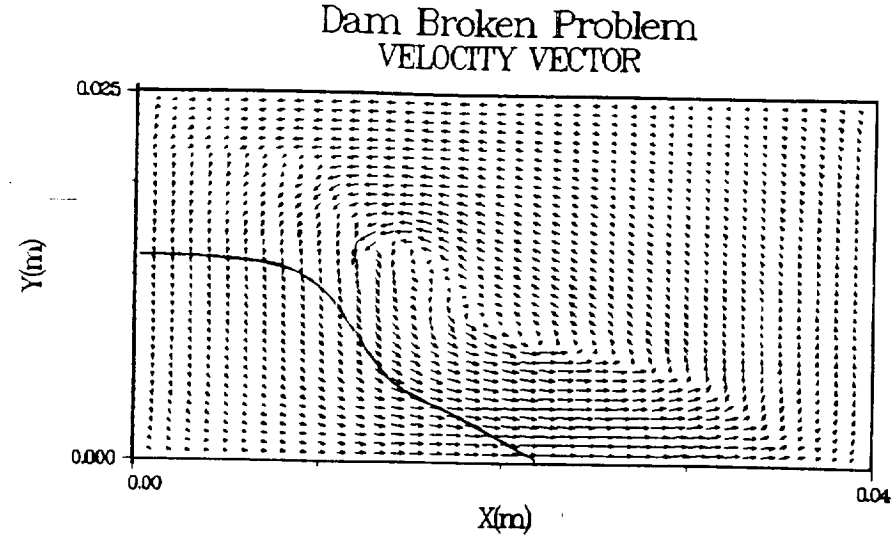

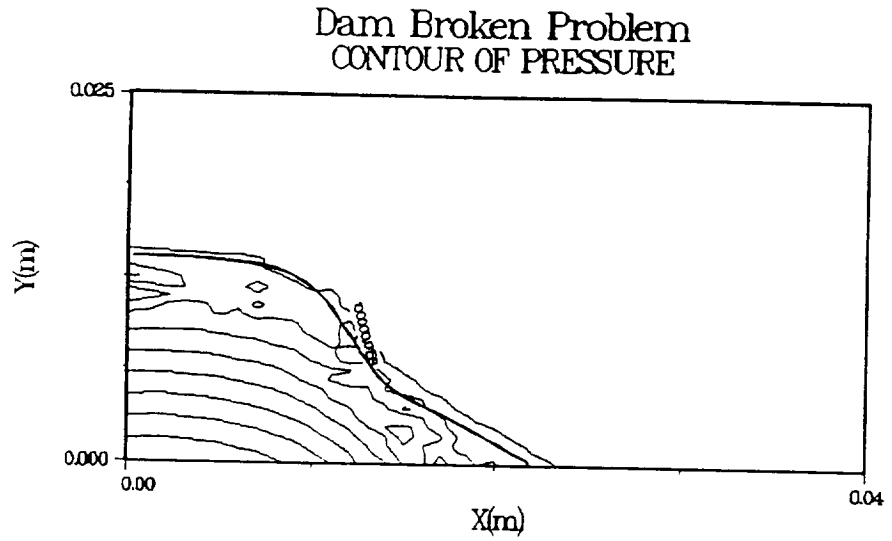

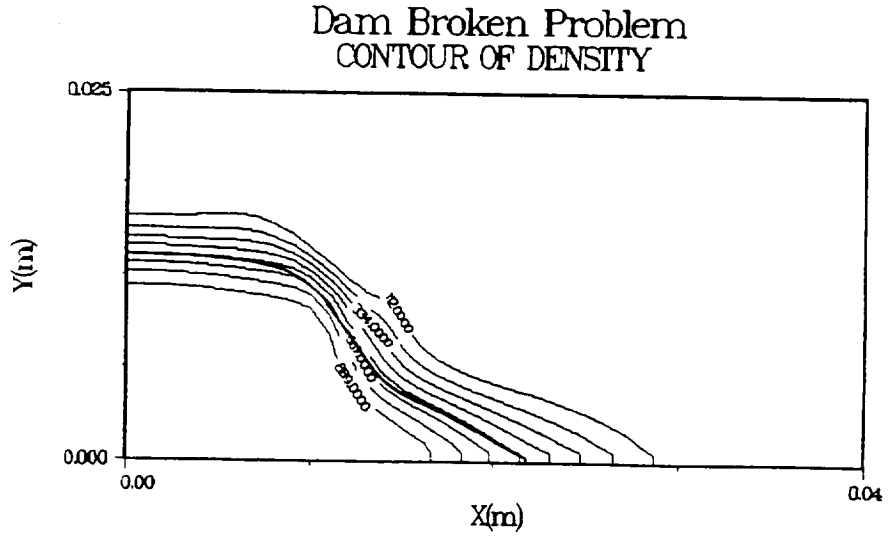

Fig. 4 Continue (at time = 1.4 sec)

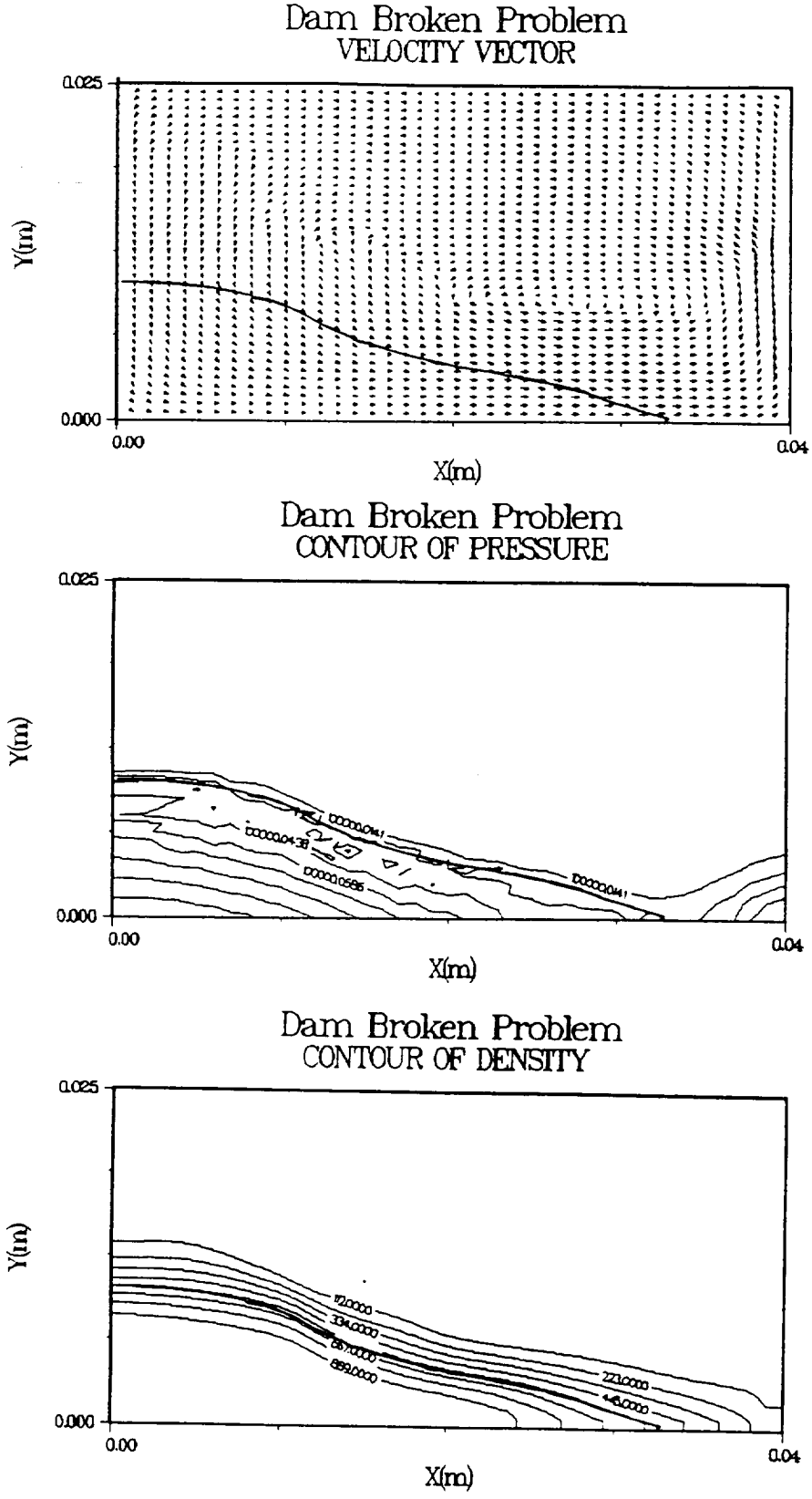

Fig. 4 Continue (at time = 2.0 sec)

5-2 . Water Sloshing Problem

The second test calculation is that of liquid water sloshing in two-dimensional rectangular tank as shown Fig. 5. The tank is left-half filled with liquid water and right-half filled with gas. At the initial state, the pressure is uniform at the value P_0 and the velocity is zero. And also, VOF value at the left-half side is equal to unity and the right-half side is zero. And the physical properties is listed in Table 3.

The numerical results are shown in Fig. 6. In this case, no analytic solution is available. However, the numerical results clearly show the qualitative sloshing behavior

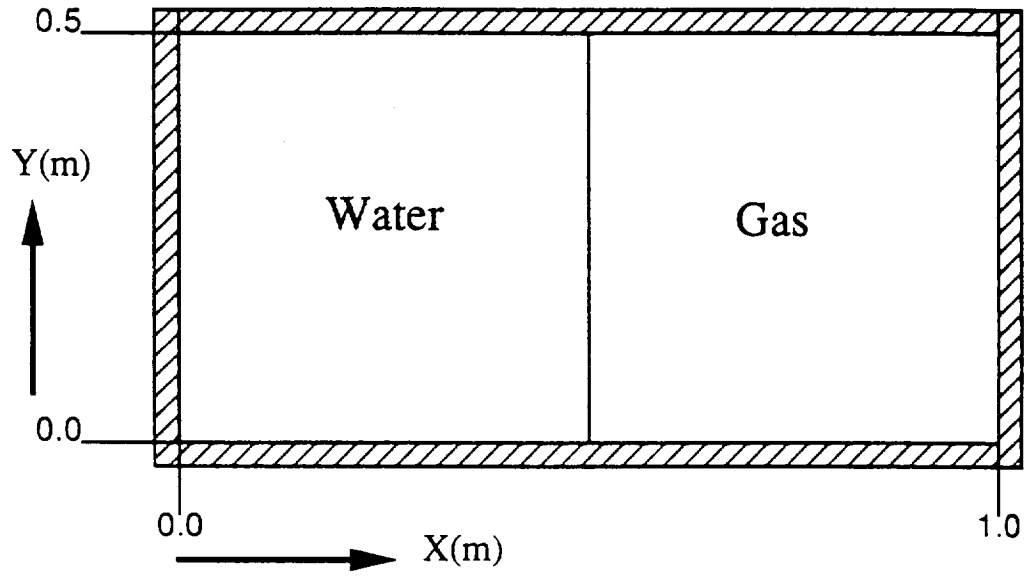

Fig. 5 Schematic diagram for water sloshing problem

which would be expected intuitively. At the beginning state, the water front starts to collapse due to the gravity force. As the water front starts to move from left to right, the gas velocity was induced due to the momentum transfer from the liquid phase (water). And also the

Table 3. The physical properties for the water sloshing problem

o Liquid physical properties			
	density	: 960.0	K_g/m^3
	viscosity	: 1.0 E-3	K_g m/sec
o Gas physical properties			
	density	: 0.585	K_g/m^3
	viscosity	: 1.8 E-5	K_g m/sec
o Gravity		: 9.8	m/sec^2
o Initial Pressure		: 1.0	bar

recirculating flow was induced. The numerical results are compared with ref. [30] with close agreement qualitatively.

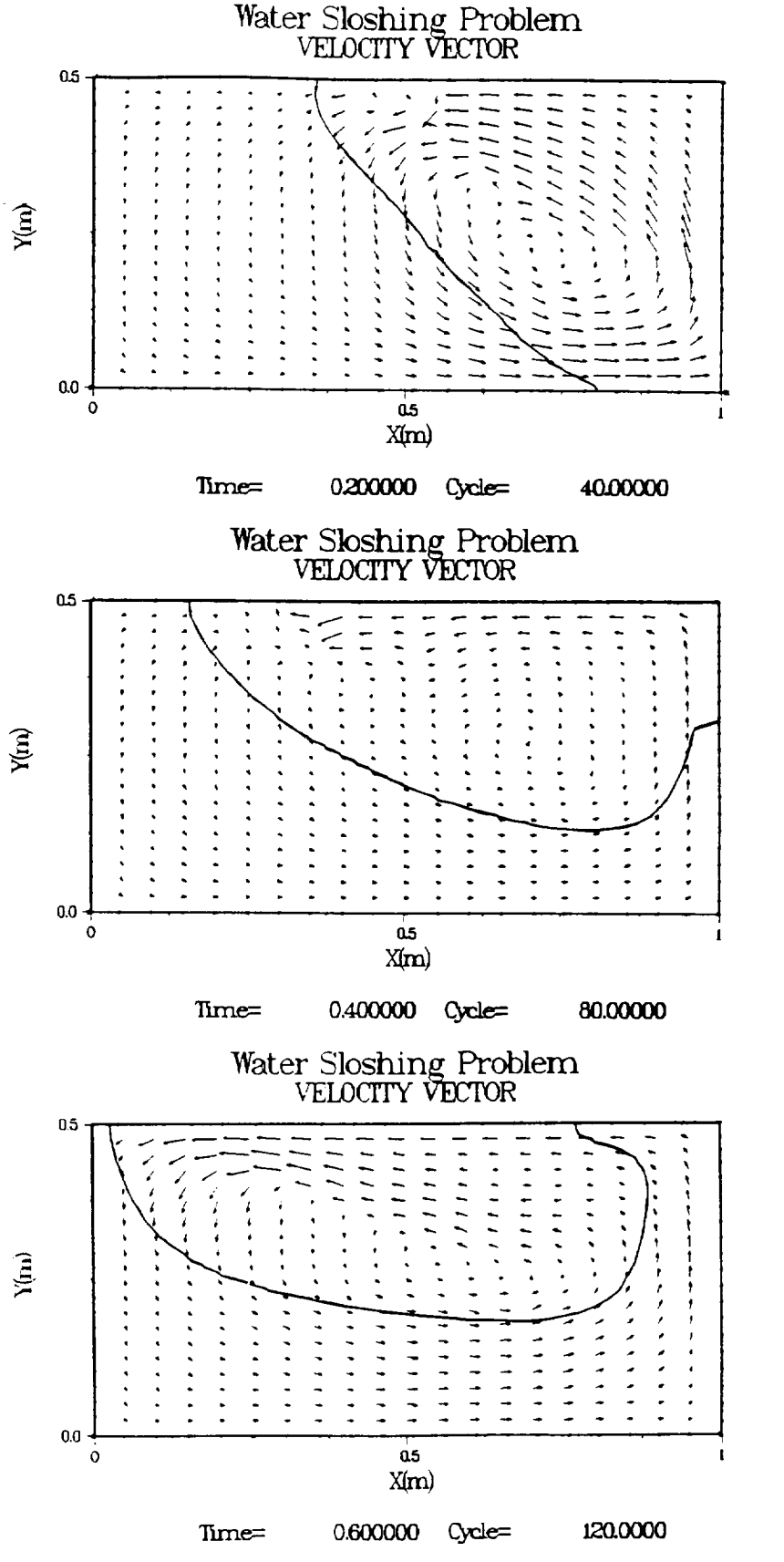

Fig. 6 Velocity vector and free surface configuration computed for water sloshing problem

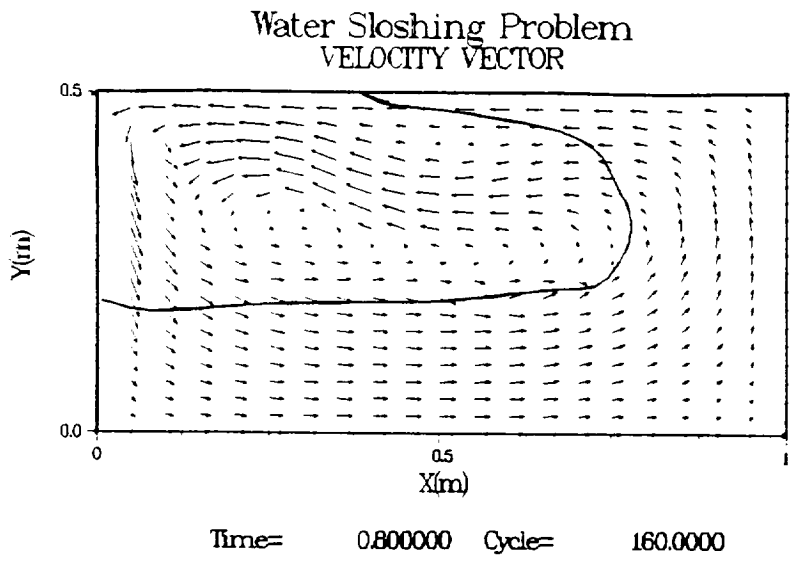

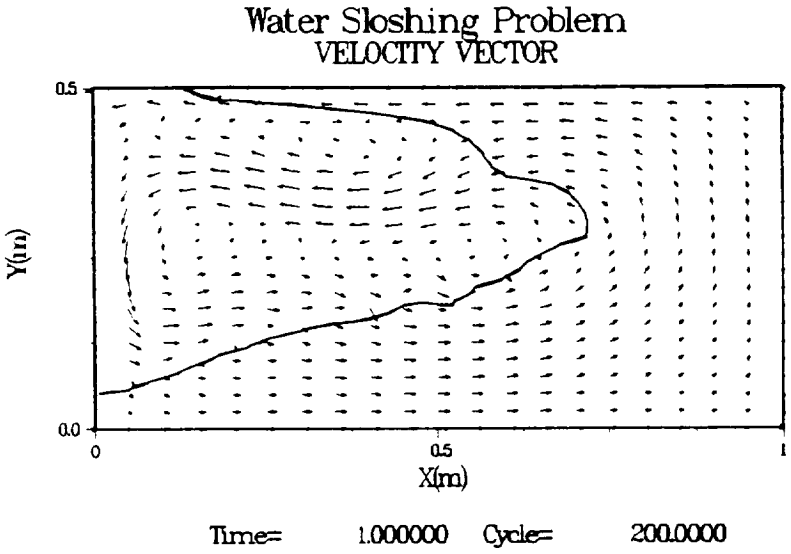

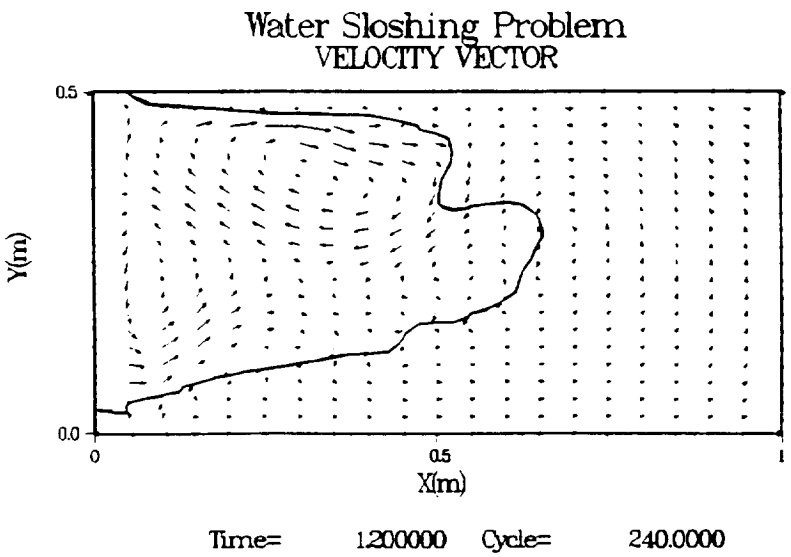

Fig. 6 Continue

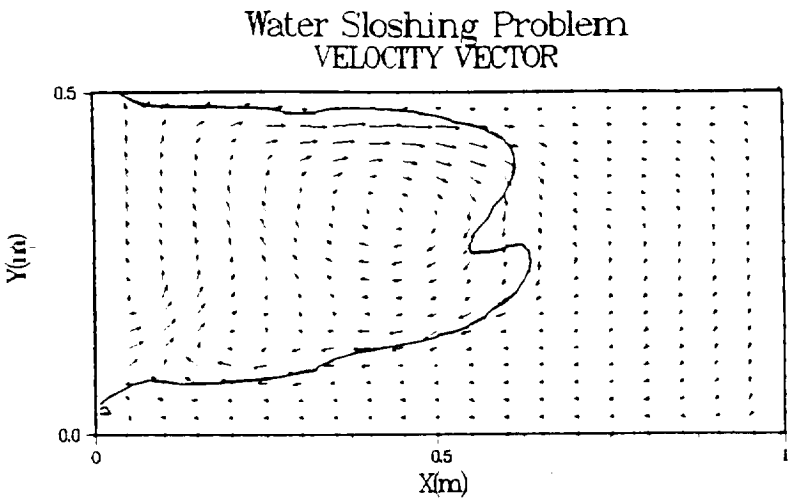

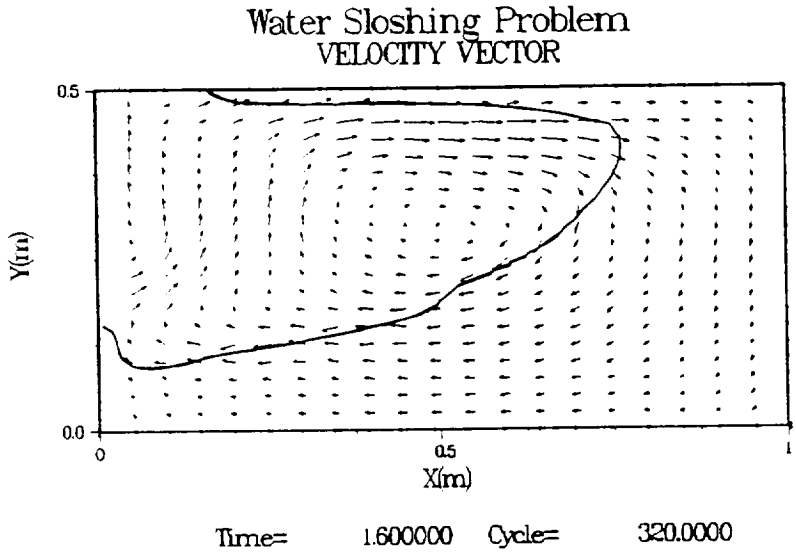

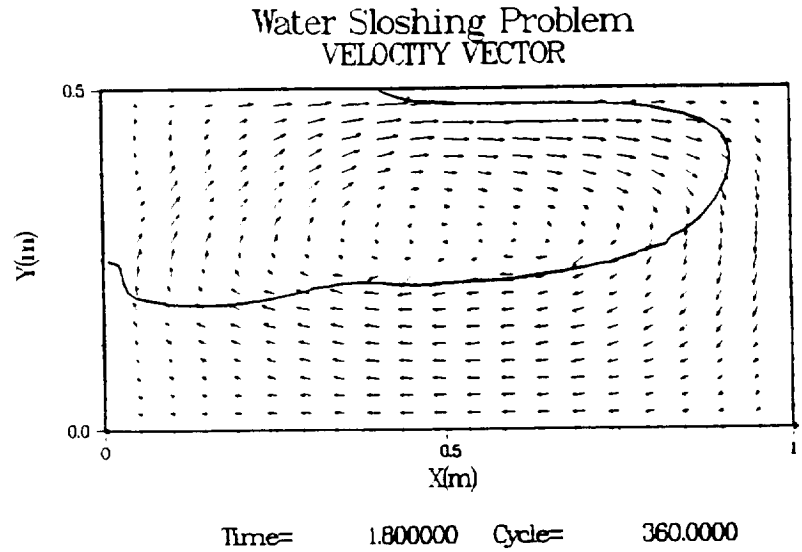

Fig. 6 Continue

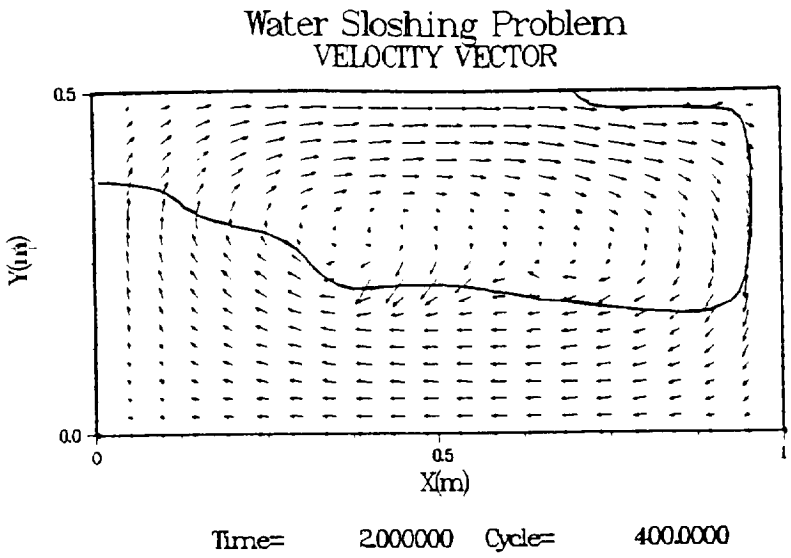

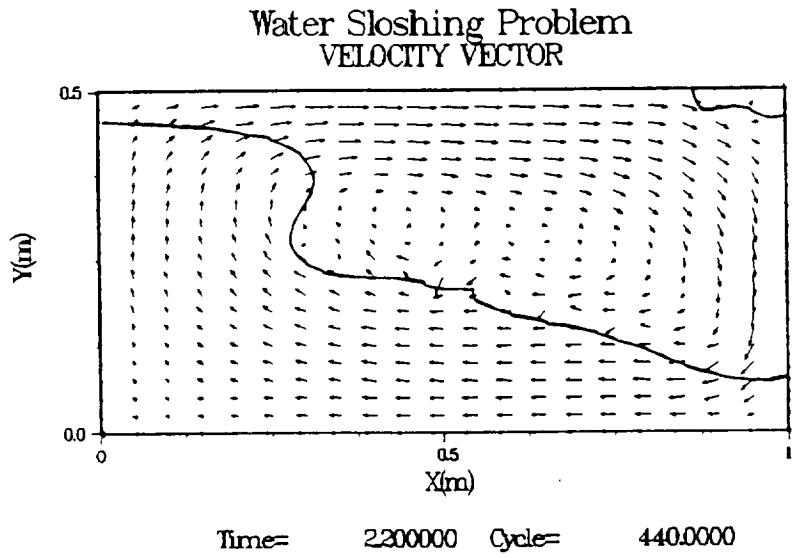

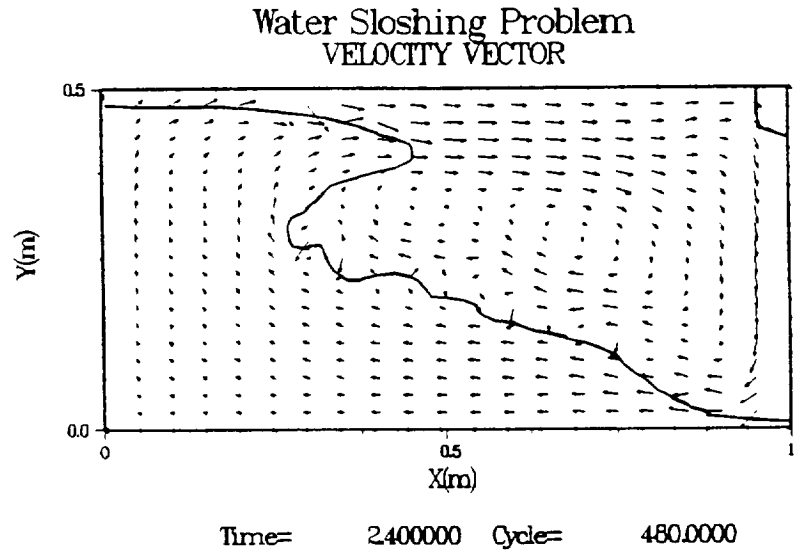

Fig. 6 Continue

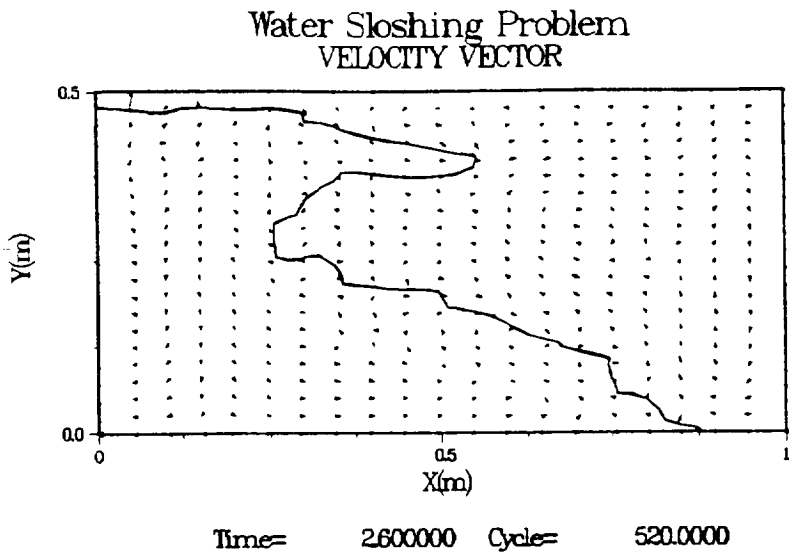

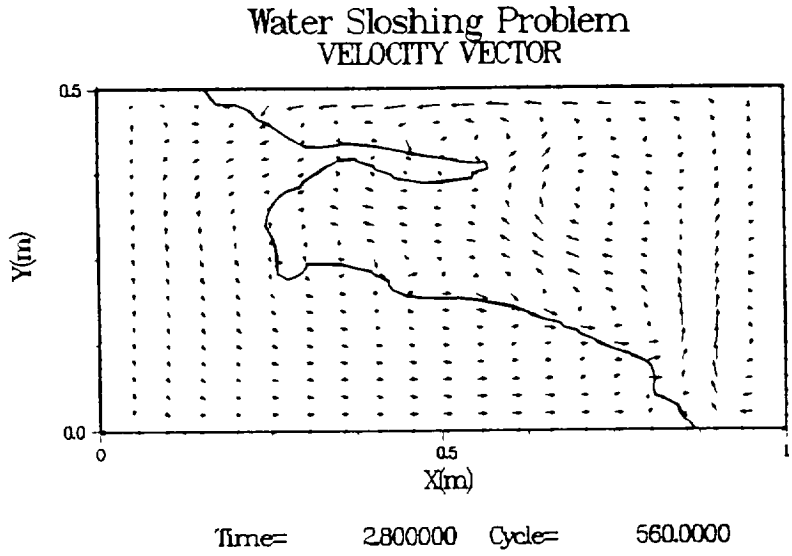

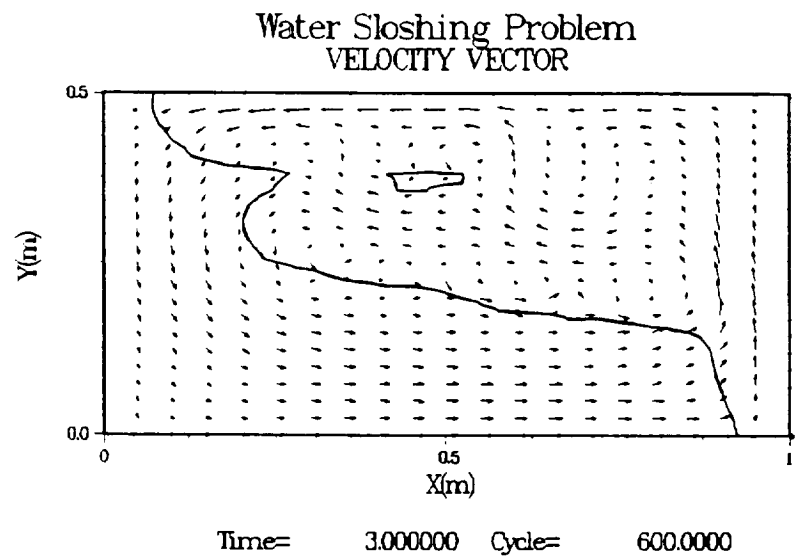

Fig. 6 Continue

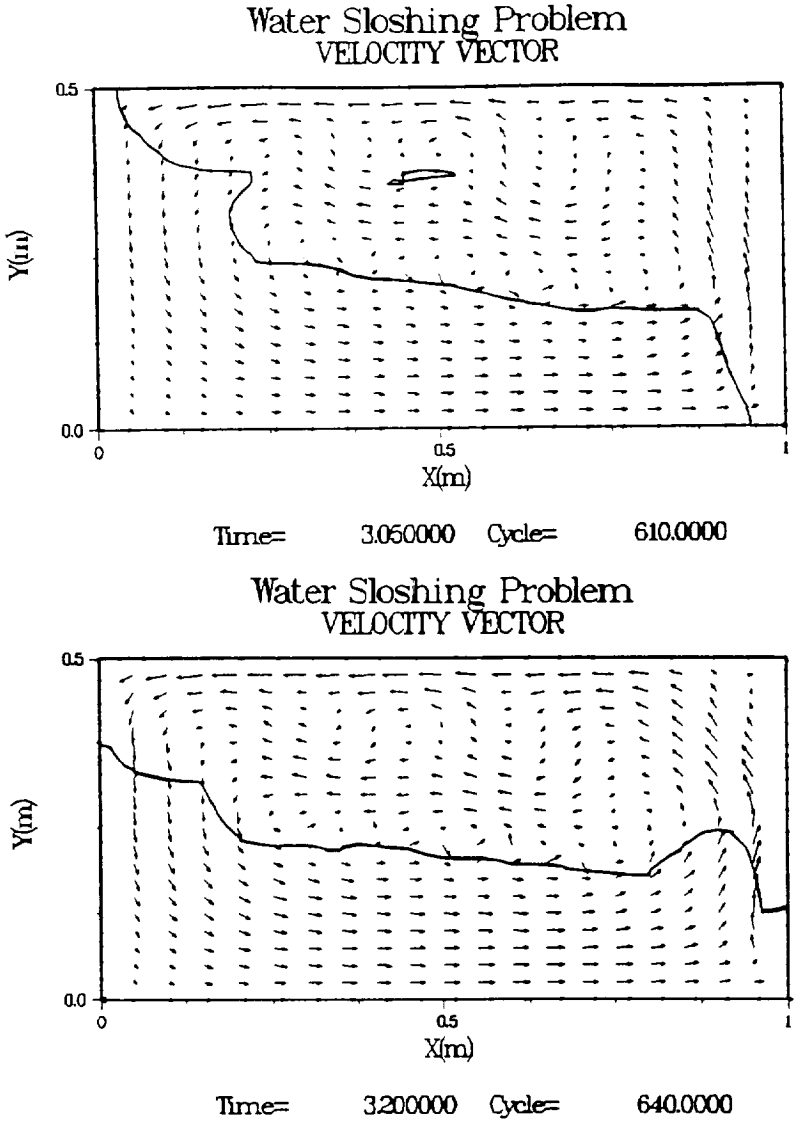

Fig. 6 Continue

5-3. Equilibrium Droplet Problem

To test the surface tension force, the equilibrium droplet problem was chosen. In this problem, the viscous, gravitational, or other external forces were not considered. Only the surface tension effect is considered. Therefore, this surface tension causes a static liquid drop to become spherical.

For numerical solution, the Cartesian geometry using a two-dimensional 0.06 x 0.06 (m) computational domain is chosen as shown in Fig. 7. Also, a regular, orthogonal grid with uniform mesh is used The physical properties are listed in Table 4 and the radius of droplet is 0.02 m. This droplet is located at the center on computational domain (0.03m x 0.03m).

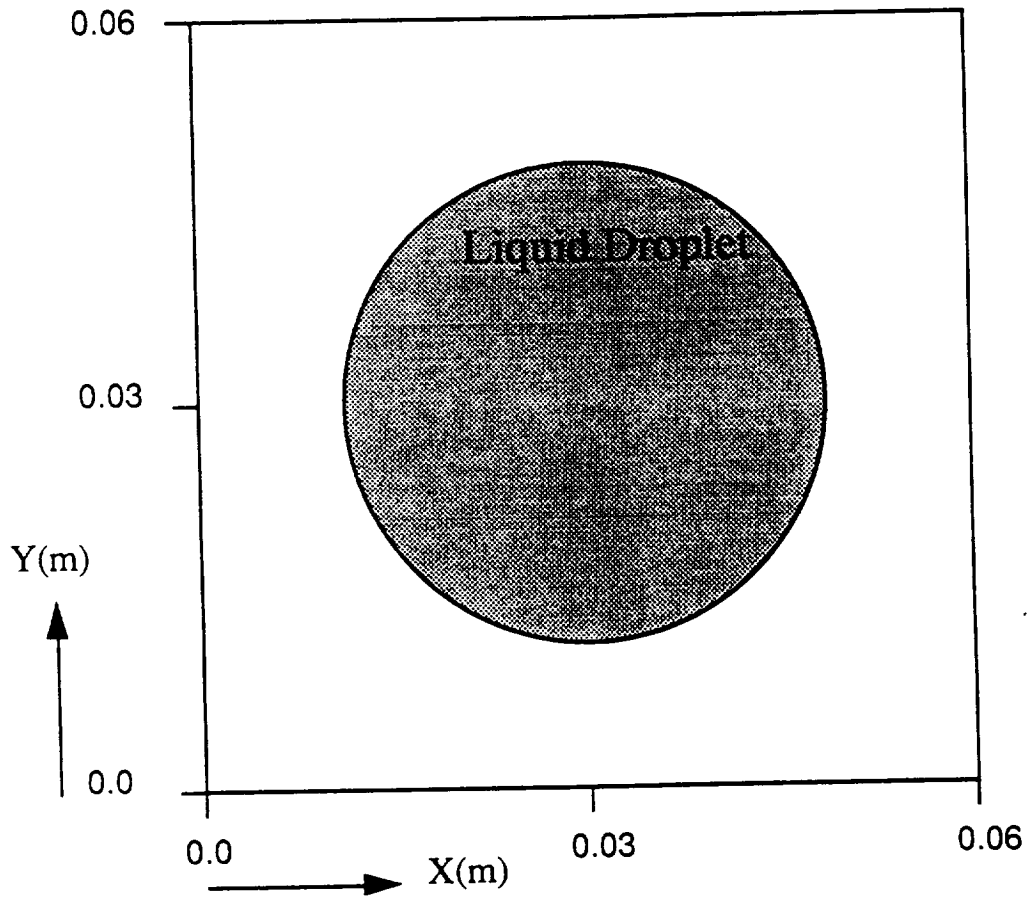

Fig. 7 Schematic diagram for equilibrium droplet problem

Table 4. The physical properties for the equilibrium droplet problem

o Liquid physical properties			
density	:	1000.0	Kg/m^3
surface tension coefficient	:	0.02361	N/m
initial radius	:	0.02	m
o Gas physical properties			
density	:	1.0	Kg/m^3
o Gravity	:	0.0	m/sec^2

Fig. 8 shows the numerical results, the gradient of F has its greatest magnitude in the transition region and falls to zero outside the transition region. It means that the value of mean curvature are local to the interfaces between two fluids. To calculate the surface tension, the effects of surface tension should be confined to the neighborhood of the interface. Because the surface tension is the boundary phenomena. In Fig. 8, it is seen that the velocity vectors inside the droplet are in equilibrium. Therefore, the static liquid droplet keeps spherical. Also, the surface force vector and the contour of the density are shown in Fig. 8. The results were obtained without any smoothing treatment as described in ref. [23].

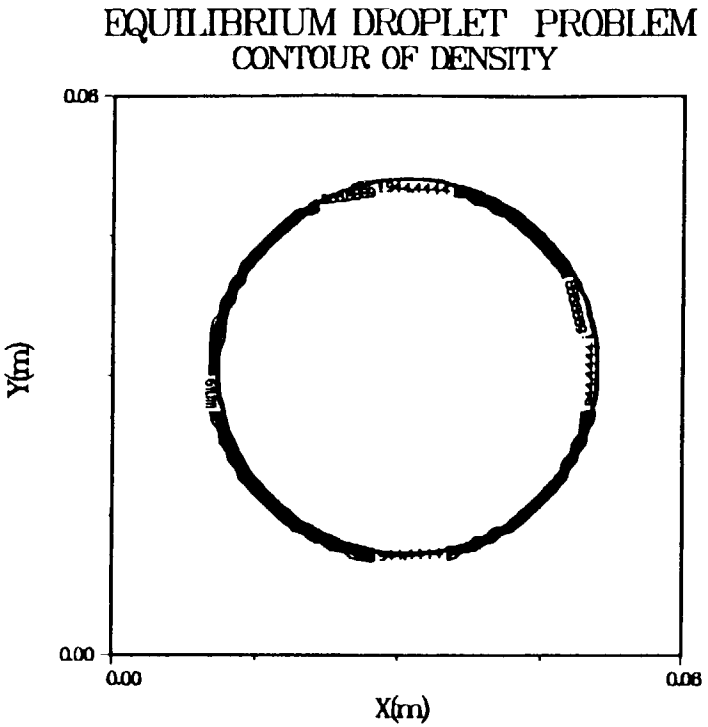

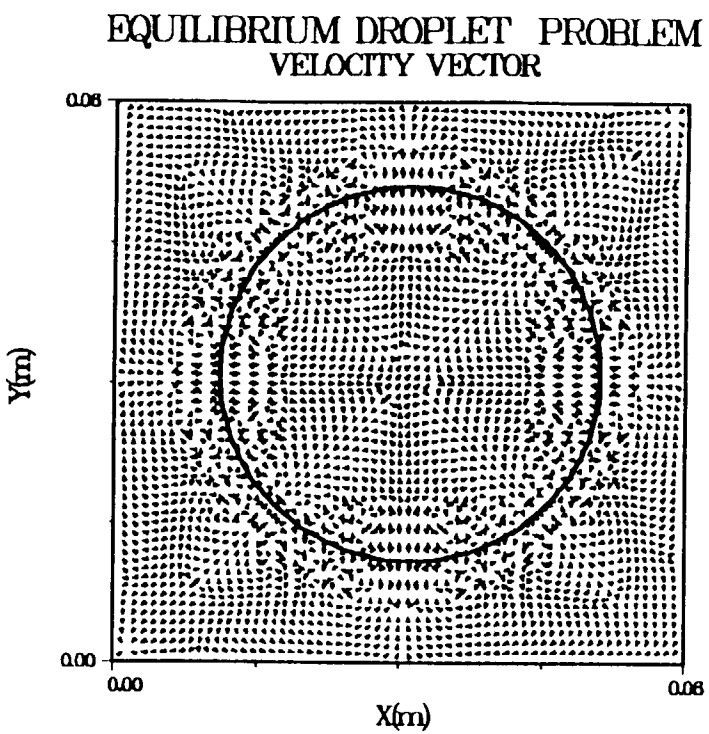

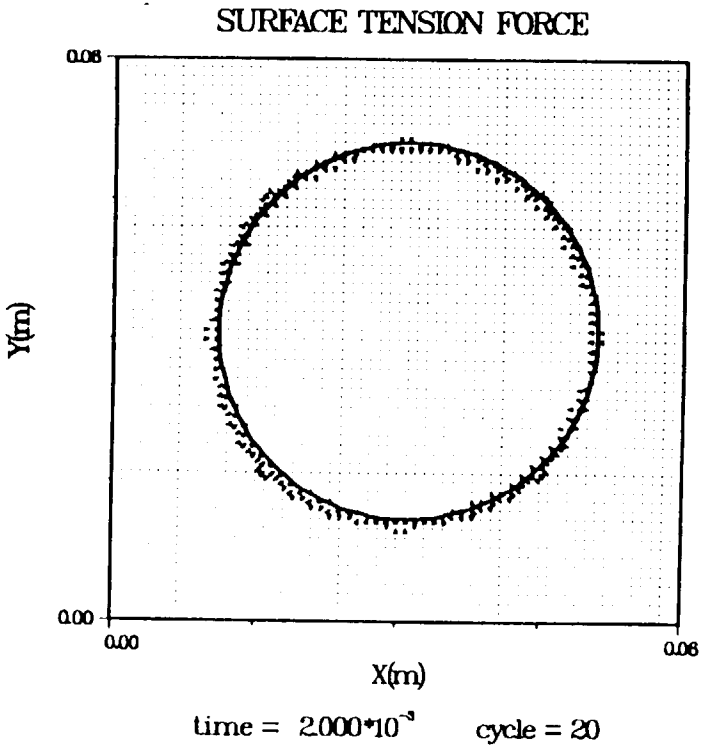

Fig. 8 Computational results

for equilibrium droplet problem

5-4. Liquid Column Instability Problem

This problem concerns the instability of a cylindrical column of fluid and a perturbation by radial displacements. A cylindrical liquid column 1.4 cm long by 0.1 cm radius was covered by a 1.4 cm long and 0.3 cm calculation domain with a 232 x 101 grid. Liquid to background fluid density ratio is approximately 2 and surface tension coefficient 59.0 dynes/cm is modeled.

The interfaces between two immiscible is initially perturbed by a cosine function with an amplitude of 0.01 R_O (liquid column radius). For large amplitude displacements, the non-linearity takes effect and the liquid column deforms and pinch-off occurs to form small satellite drops between the large drops. Details of the satellite drop formations are very sensitive to the grid system and topological reconstructions of VOF data into the breaking up of liquid bulges. A series of computational results of the free surface and velocity filed are shown Fig. 9 depicting the deformation of the liquid column into droplets. This computational results are compared to experimental results of [31] shown in Fig.10.

Next, a cylindrical liquid column 1 cm long by 0.05 cm radius was covered by a 1 cm long and 0.15 cm calculation domain with a 81 x 31 grid. Liquid to gas density ratio is approximately 1000 and surface tension coefficient 72.8 dynes/cm is modeled. The gas-liquid interface is initially perturbed by a cosine function with an amplitude of 0.001 a (liquid column radius). The normalized perturbation growth plotted in Fig. 11 vs. non-dimensional time is compared with the linear theory of Rayleigh. The current results compared favorably with the linear theory as well as with other results by SOLA-VOF [25] and ARICC-ST code [13].

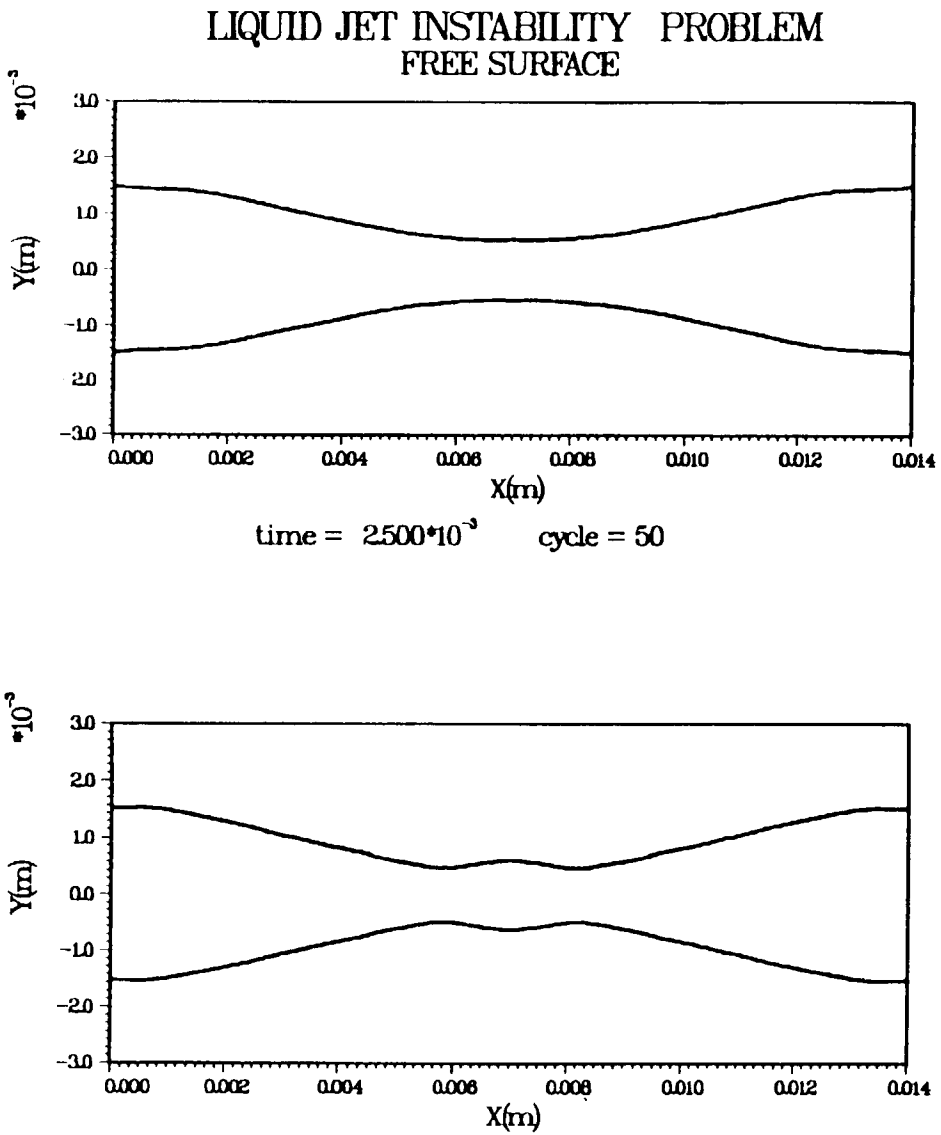

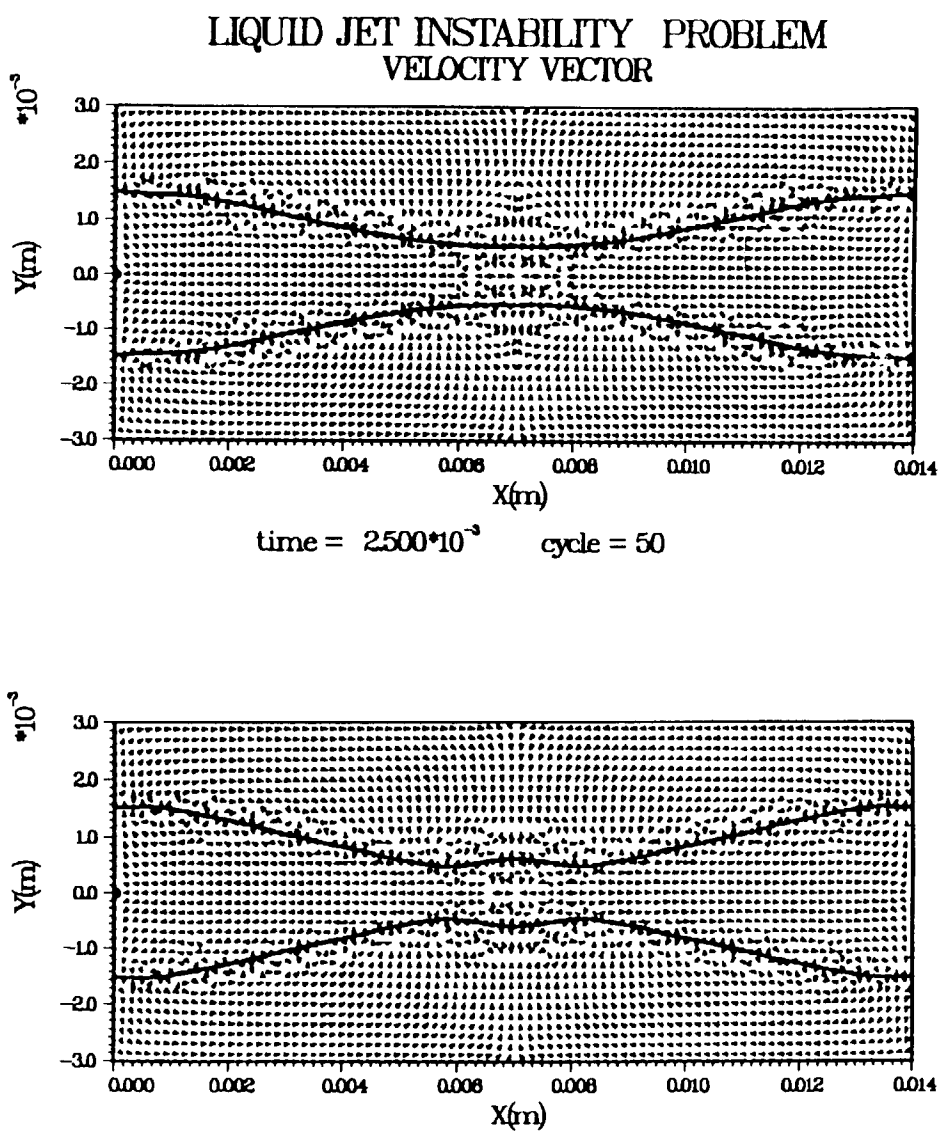

Fig. 9 Velocity vector and free surface configuration computed for liquid jet instability problem

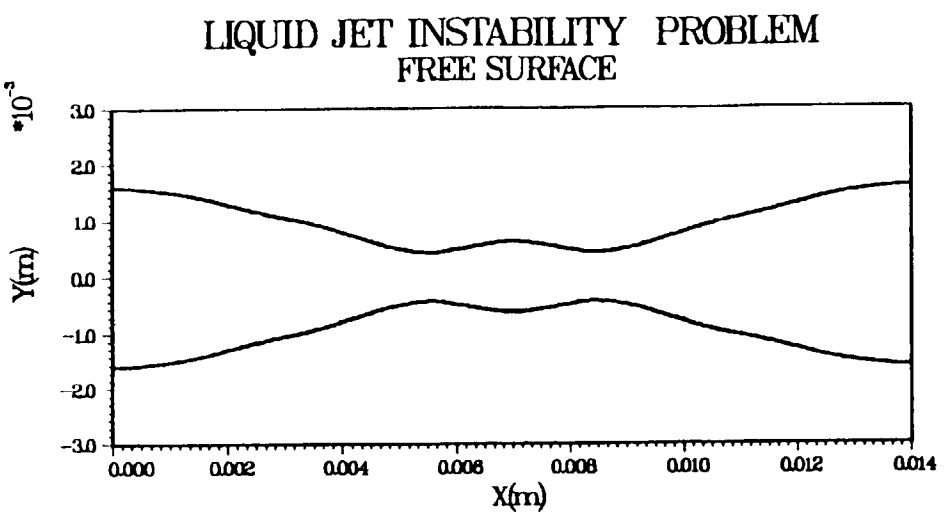

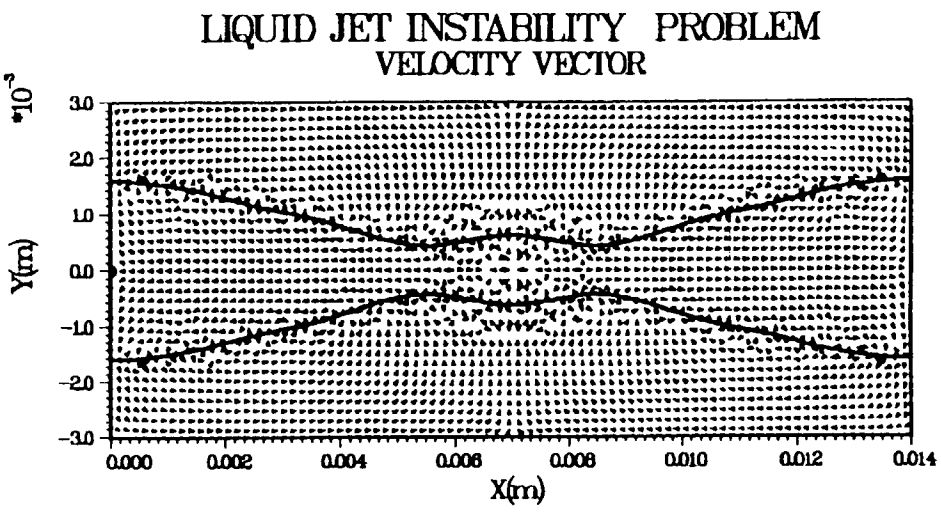

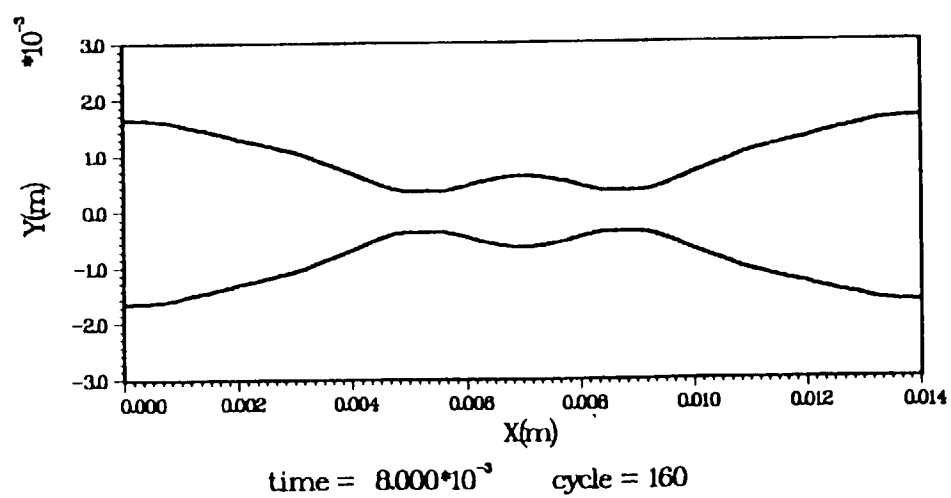

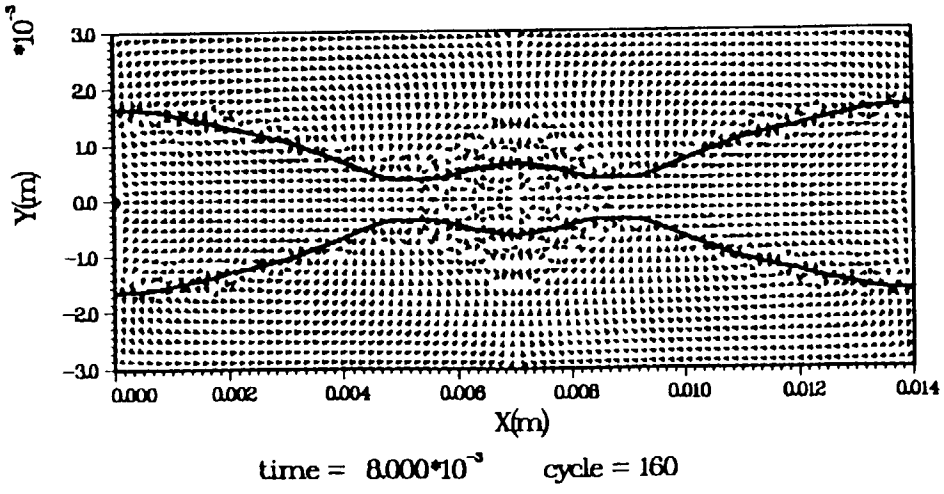

Fig. 9 Continue

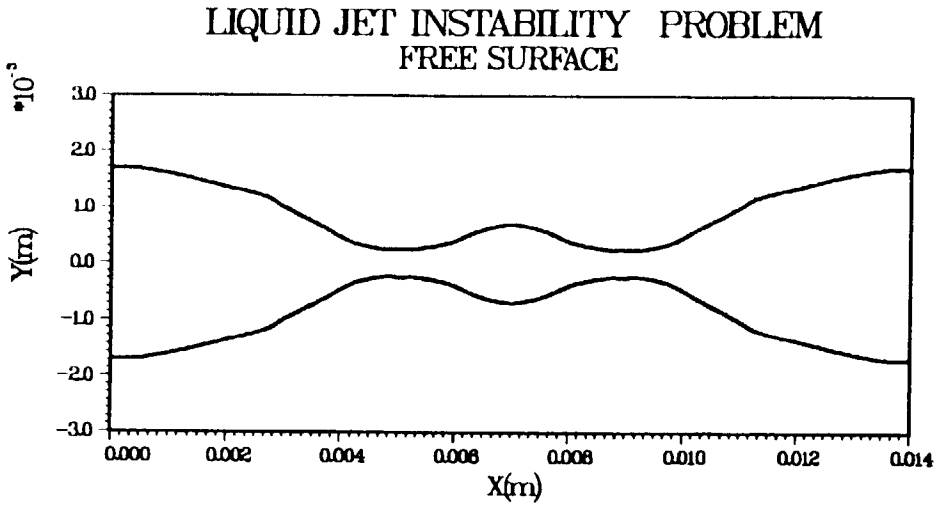

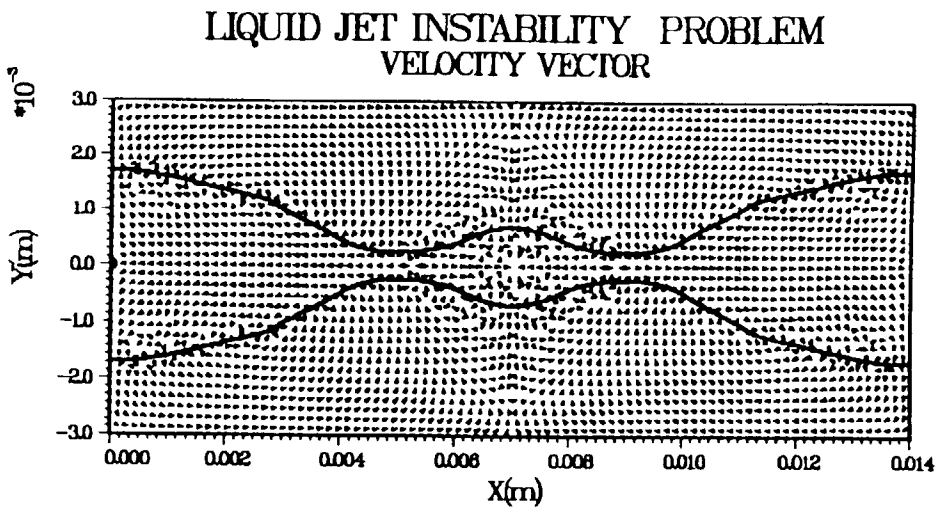

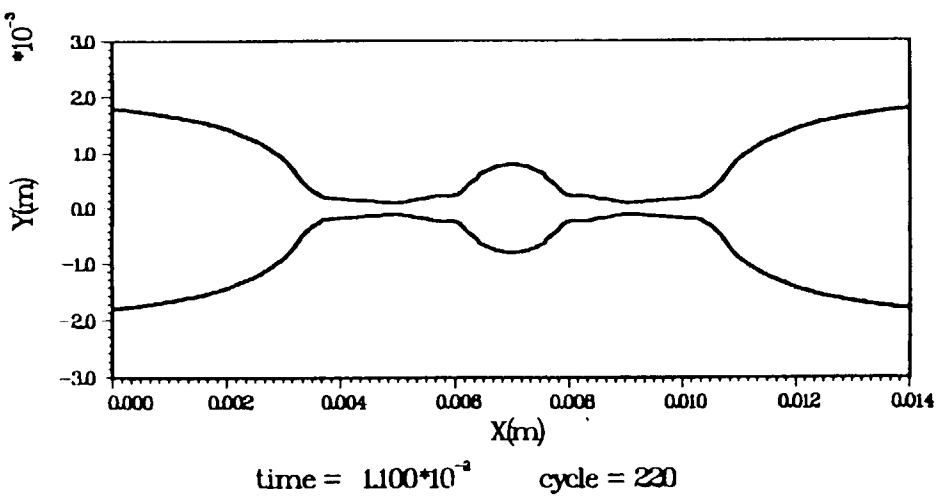

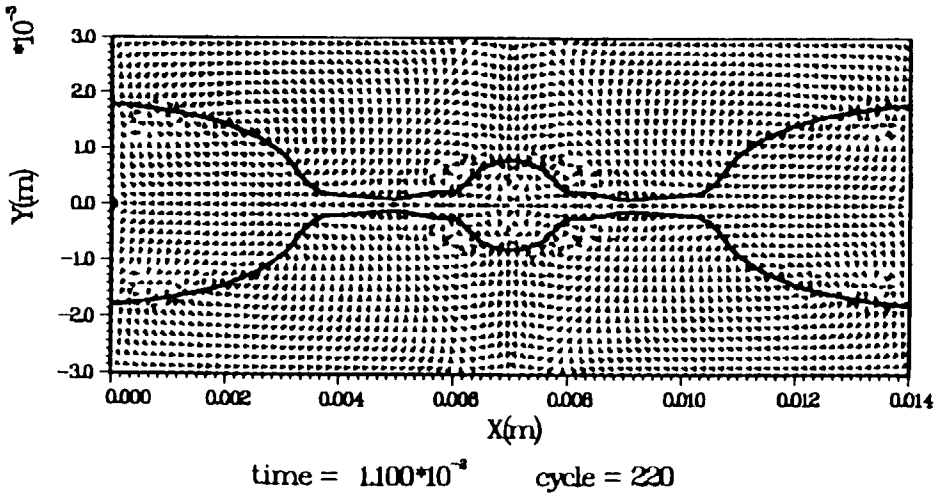

Fig. 9 Continue

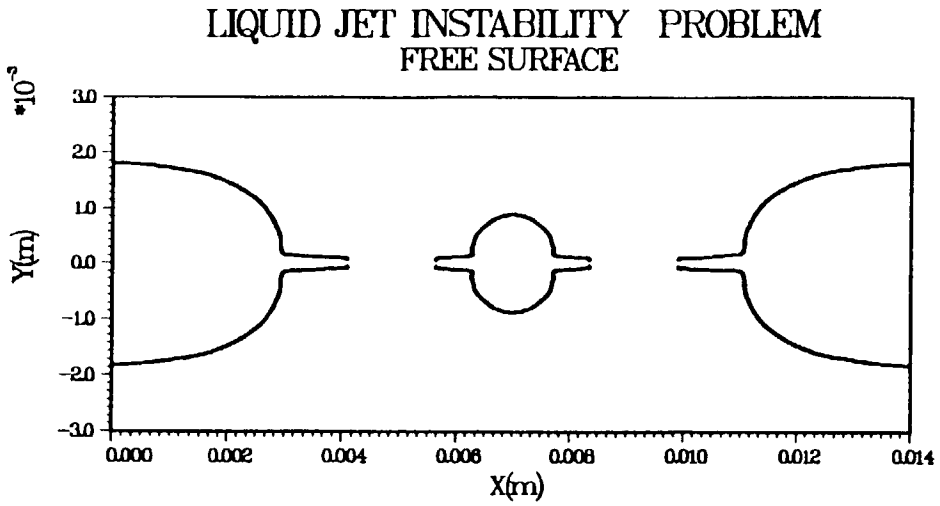

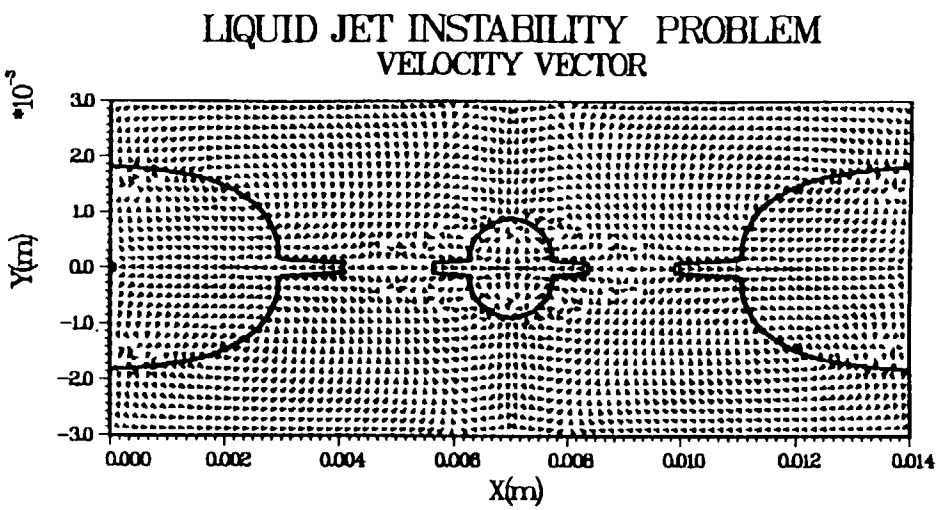

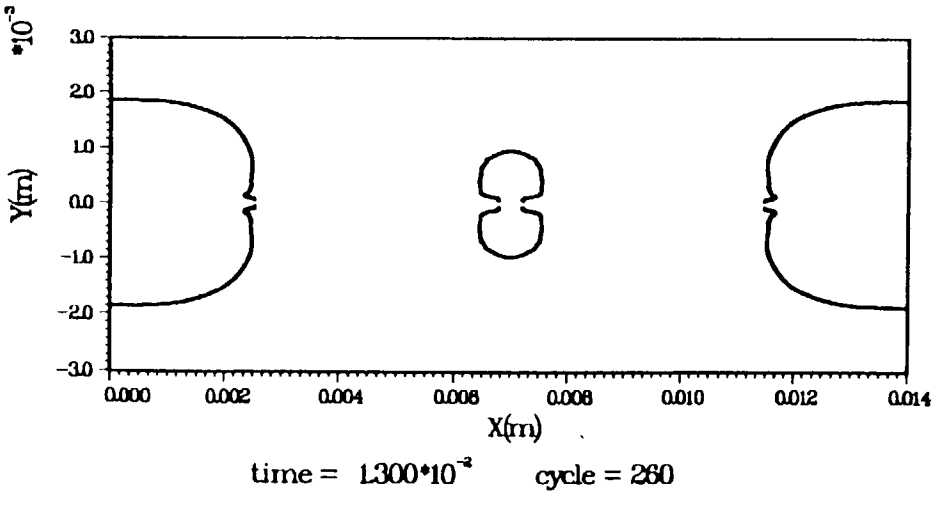

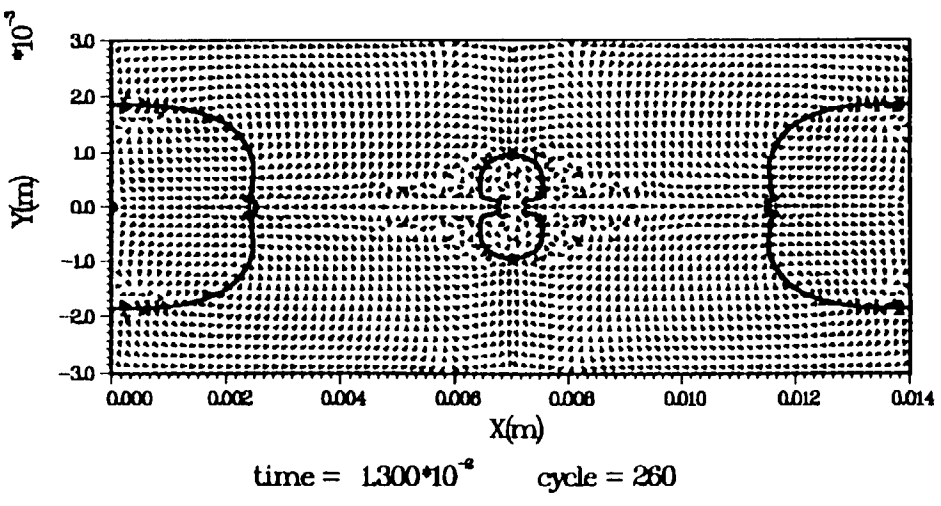

Fig. 9 Continue

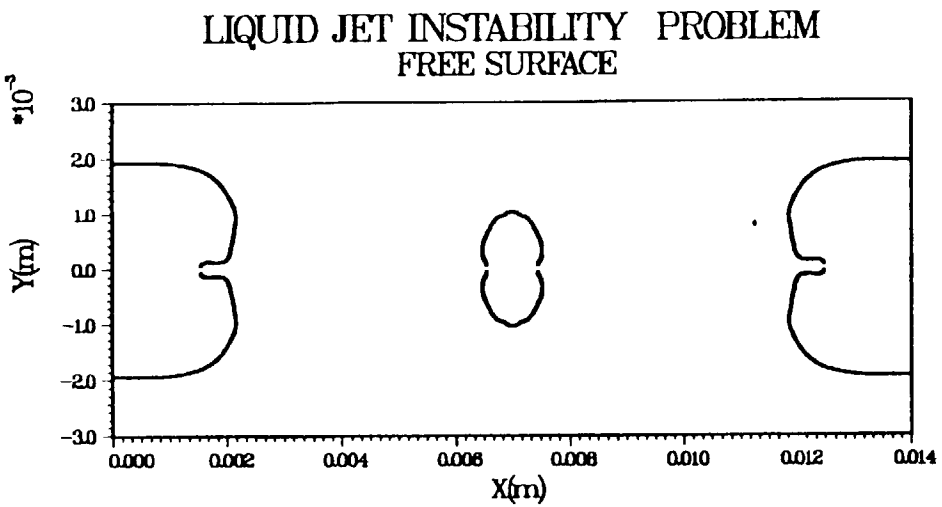

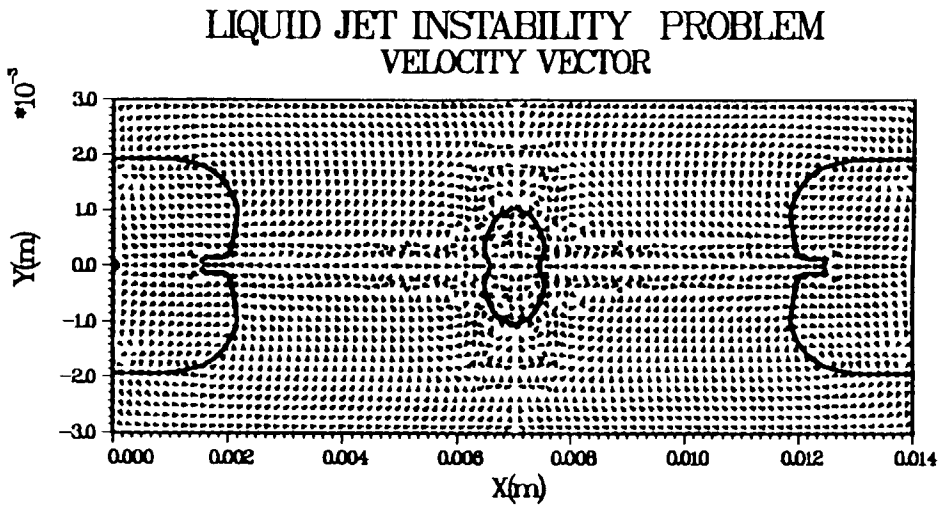

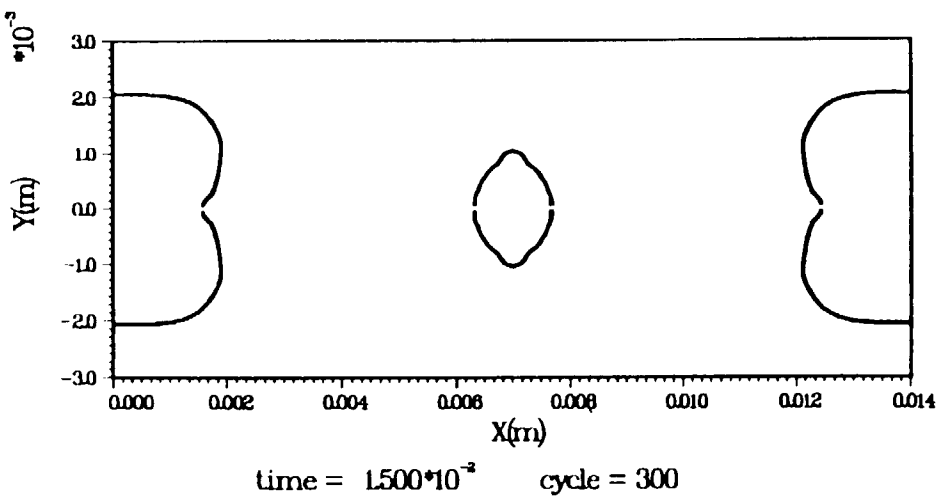

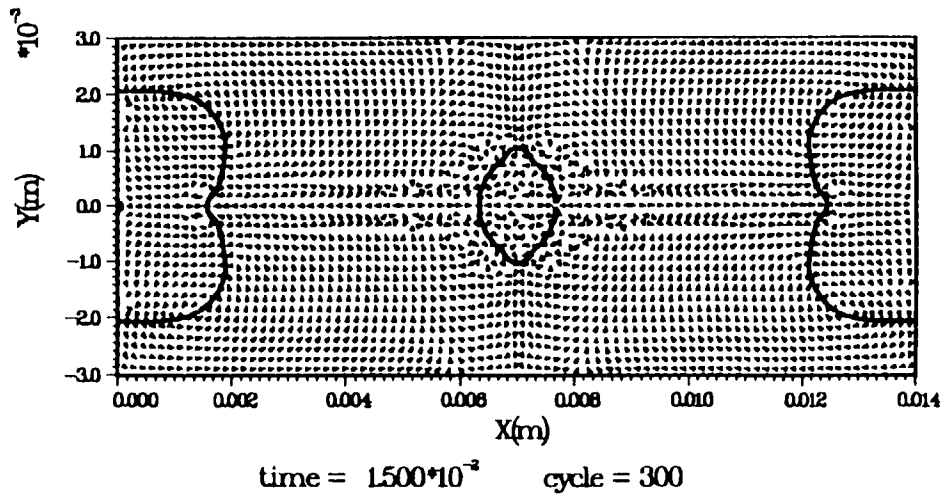

Fig. 9 Continue

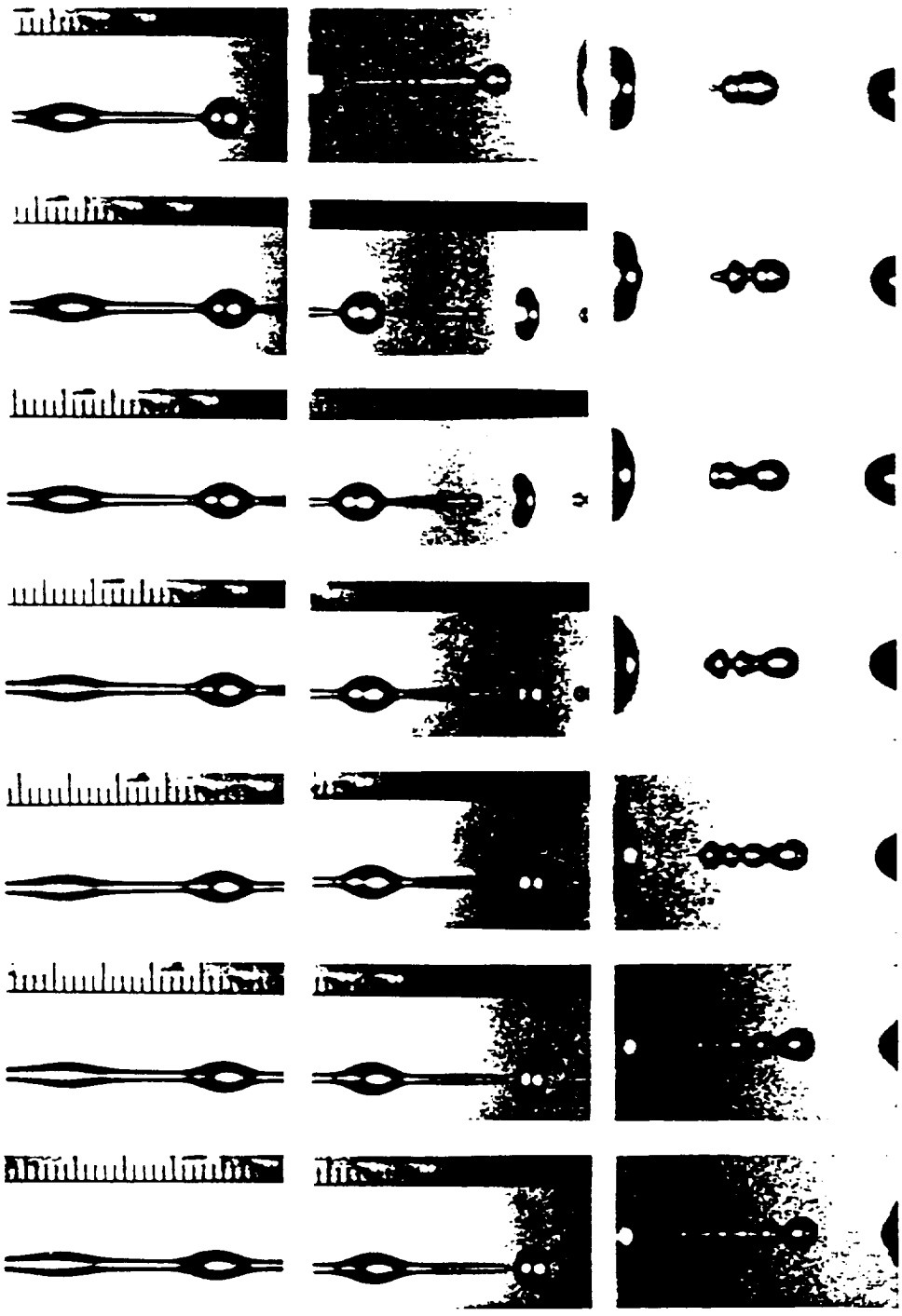

Fig. 10 Experimental results of water jet breakup with σ = 59 dynes/cm.
Time interval between each photograph is 1.25×10^{-3} sec.
(time increases from left to right, top to bottom)

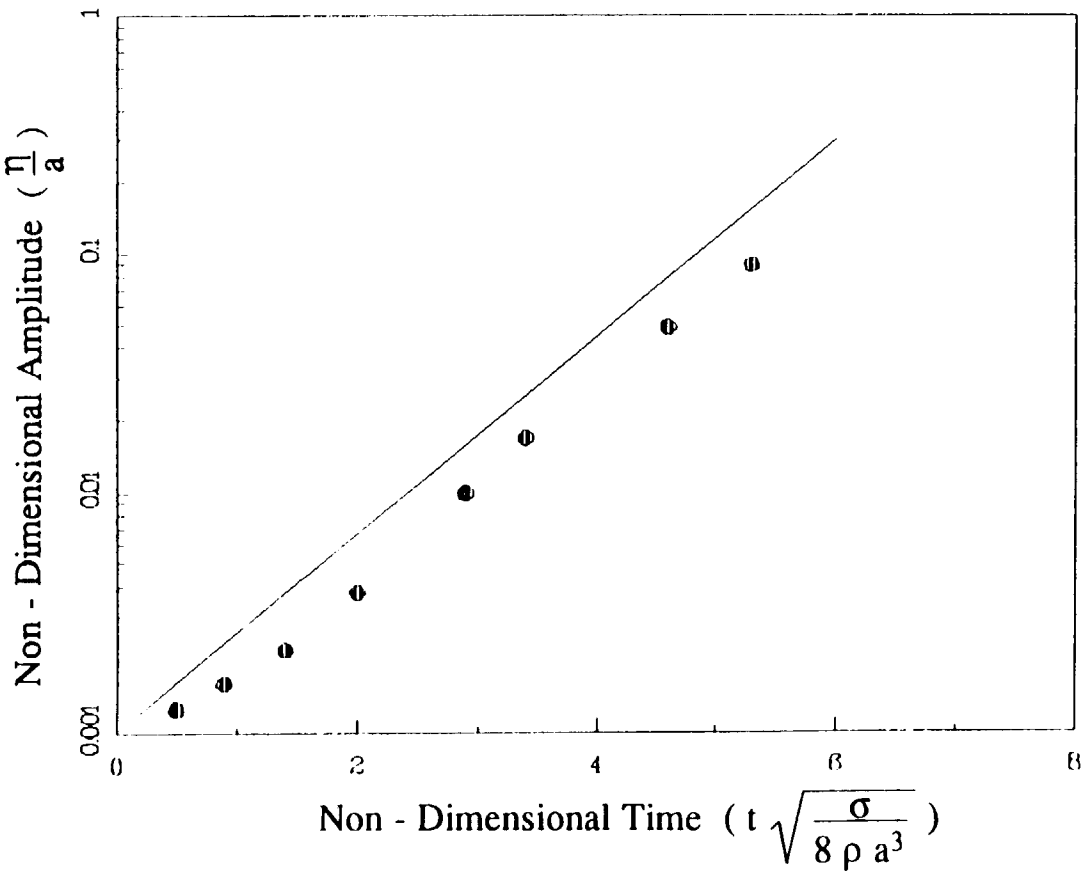

Fig. 11 Comparison of numerical results to linear theory for the liquid column instability problem (——— : linear theory, • : numerical results)

6. Conclusion and Recommendation

The development of a combined Eulerian-VOF-Lagrangian method has been initiated based on a pressure-based transient gas-droplet solution procedure [28]. This study concentrated on implementing the VOF method and CSF model into the solver for sharp interface tracking and efficient handling of the surface tension force. Validation studies indicated that the current methodology can readily be extended to incorporate other physical submodel such as compressibility effects in the gas phase, spray tracking and turbulence for atomization process simulation.

The future work for the next phase studies should include:

1. Determine the onset of primary breakup using the VOF data and develop an criterion coupling with Lagrangian droplet tracking.
2. Interfacial transport phenomena including heat effects.
3. Interfacial transport due to turbulence effects.
4. Extension to three-dimensional multi-jet simulations. This will involve extending the VOF method to couple with multi-zone unstructure grid methods.

7. References

1. Combs, L. P., and Schuman, M. D.,"Steady State Rocket Combustion of Gaseous Hydrogen and Liquid Oxygen," Research Report No.64-29, Rocketdyne, March, 1965.

2. Elkotb, M. M.,"Fuel Atomization for Spray Modeling ," Prog.Energy Combustions Sci., Vol.8, pp. 61-91, 1982.

3. Mayer, E., "Theory of Liquid Atomization in High Velocity Gas Streams," ARS J.,Vol.16, pp. 2052-2055, 1973.

4. Leib, S. J., and Goldstein, M. E., "Convective and Abosolute Instability of a Viscous Liquid Jet," Physics of Fluids, Vol.29, pp. 952-954, 1986.

5. Reitz, R. D., "Modeling Atomization Processes in High Pressure Vaporizing Sprays," Atomization and Spray Tech., Vol.3, pp. 309-337, 1987.

6. Reitz, R. D., and Diwaker, R., "Structure of High Pressure Fuel Spray," SAE Paper 870598, 1987.

7. Kim, Y. M., Shang, H. M., Chen, C. P., Ziebarth, J. P., and Wang, T. S., "Numerical Studies of Dilute and Dense Spray Characteristics," AIAA-92-0225, 1992.

8. Kim, Y. M., Chen, C. P., and Ziebarth, J. P., "Numerical Simulation of Combustion Instability in Liquid-Fueled Engines," AIAA-92-0775, 1992.

9. Kim, Y. M., Shang, H. M., and Chen, C. P., " Non-Isotropic Turbulence Effects on Spray Combustion," AIAA-91-2196, 1991.

10. Habiballah, M., Lourme, D., and Pit, F., "PHEDRE-Numerical Model for Combustiion Stability Studies Applied to the Ariane Viking Engine," J. Propulsion and Power, pp. 322-329, 1991.

11. Cheuch, S., Przekwas, A., Yang, H. Q., and Gross, K., "Direct Simulation for the Instability and Breakup of Laminar Liquid Jet," AIAA-90-2066, 1990.

12. Liang, P. Y., Jensen, R. J, and Chang, Y. M., " Numerical Analysis of SSME Preburner Injector Atomization and Combustion Processs ," AIAA-86-0454, 1986.

13. Liang, P. Y., and Ungewitter, R., " Direct Numerical Simulation of Atomization and Free Surface instability from First Principles," JANNAF 27th Combustion Subcommittee Meeting, Vol. 3, pp. 239-252, Nov., 1990.

14. Liang, P. Y., and Schuman, M. D., "Atomization Modeling in a Multi-phase Flow Environment and Comparison with Experiments," AIAA-90-1617, 1990.

15. Liang, P. Y., and Ungewitter, R., "Multiphase Simulation of Coaxial Injector Combustion," AIAA-92-0345, 1992.

16. Liang, P. Y., and Chan, D. C., "Development of A Robust Pressure Based Numerical Scheme for Spray Combustion Applications," AIAA-93-0902, 1993.

17. Chen, Z. J., Chen, C. P., and Chen, Y. S., "A pressure Correction method for Calculation of Compressible Chemical Reacting Flow," AIAA-92-3012, July, 1992.

18. Jiang, Y., Chen, C. P., and Shang, H. M., "A New Pressure-Velocity Coupling Procedure for Invicid and Viscous Flows at All Speeds," 4th Int. Sym. on CFD U.C. Davis, Sep. 9-12, pp. 545-550, 1991.

19. Shang, H. M.,"Numerical Studies of Spray Combustion in Liquid-Fueled Engines," Ph.D. Dissertation, University of Alabama in Huntsville, Dec. 1992.

20. Chen ,C. P., Jiang, Y., Kim, Y. M., and Shang, H. M., "A Computer Code for multiphase All-Speed Transient Flows in Complex Geometries," NASA Contractor report, NAG8-092, Oct., 1991.

21. Chakravarthy, S. R., and Osher, S., "A New Class of High Accuracy TVD Schemes for Hyperbolic Conservation Laws," AIAA-85-0363, Jan., 1985.

22. Kothe, D. B., Mjolsness, R. C., "RIPPLE: A New Model for Incompressible Flows with Free Surfaces," AIAA Journal, Vol.30, No.11, Nov. pp. 2694 - 2700, 1992.

23. Brackbill, J. U., Kothe, D. B., and Zemach, C., "A Continuum Method for Modeling Surface Tension," Journal of Computational Physics, Vol. 100, pp. 335 - 354, 1992.

24. Hirt, C. W., and Nicholes, B. D., "Volume of Fluid (VOF) Method for the Dynamics of Free Boundarues," Journal of computatinal Physics, Vol.39, No.1, pp. 201-225, 1981.

25. Nicholes, B. D., Hirt, C. W., and Hotchkiss, R. S., "SOLA-VOF: A Solution Algorithm for Transient Fluid Flow with Incompressible Flows with Free Surfaces," Los Alamos National Lab., LA-8355, Aug., 1980.

26. Jun, L., and Spalding, D. B., "Numerical Simulation of Flows with Moving Interfaces," PCH PhysicoChemical Hydrodynamics, Vol.10, No.5/6, pp. 625-637, 1988.

27. Issa, R. I., "Solution of the Implicitly Discretised Fluid Flow Equations by Operator-Splitting," Journal of Computatiional Physics, Vol. 62, pp. 40-65, 1985.

28. Chen, C. P., Shang, H. M., and Jiang, Y., " An Effective Pressure-Velocity Procedure for Gas-Droplet Two-Phase Flow Calculation," Int. J. Numerical Methods in Fluids, Vol. 15, pp. 233-245, 1992.

29. Martin, J. C., and Moyce, W. J., "An experimental study of the collapse of liquid column on a rigid horizontal plane," Phil. Trans. R. Soc. 244, 312, 1952.

30. Ramshaw, J. D., and Trapp, J. A., "A Numerical Technique for Low-Speed Homogeneous Two-Phase Flow with Sharp Interfaces," Journal of Computational Physics, Vol. 21, pp. 438-453, 1976.

31. Goedde, E.F., and Yuen, M.C., " Experiments on Liquid Jet Instabililty," Journal of Fluid Mechanics, Vol. 40, pp 495-511, 1970